

Reference Cavity Suspension Commissioning Of the 10 m Prototype

Sarah E. Zuraw
Physics Department,
University of Massachusetts at Amherst

International REU 2012
University of Florida

Supervisors:
Prof. Dr. Stefan Goßler, Dr. Tobin Fricke,
And Tobias Westphal
August 01, 2013

Abstract:

The 10 m prototype interferometer is currently being constructed at the AEI in Hannover, Germany. This paper discusses the details of the commissioning of the Reference Cavity suspension, one of many subsystems of the 10 m prototype. It was found during the course of the commissioning of the Reference Cavity that there is a large amount of magnetic cross talk between BOSEMs on the upper mass of the suspension. Transfer function measurements of the suspension were taken. The results showed that the magnitude of magnetic cross talk, along with other suspension commissioning issues, is non-negligible. Moving forward a correction to the control system will be created to account for the magnetic crosstalk in the BOSEMs. The Goal of the 10 m prototype is to test advanced techniques as well as conduct experiments in macroscopic quantum mechanics.

Contents

- 1 Introduction
 - 1.1 Gravitational Waves
 - 1.2 Gravitational Wave Detectors
 - 1.3 Interferometric Detectors
 - 1.4 The 10 m Prototype

- 2 Theory and practice of Optic Suspension
 - 2.1 Noise Sources
 - 2.2 Optic Suspension and Seismic Isolation
 - 2.2.1 Seismic Attenuation System
 - 2.2.2 Optic Suspension
 - 2.3 Mathematical Modeling of Single, Double and Triple pendulum Suspensions
 - 2.3.1 Introduction and Parameters
 - 2.3.2 Vertical
 - 2.3.3 Pitch and Longitudinal
 - 2.3.4 Yaw
 - 2.3.5 Sideways and Roll
 - 2.3.6 Triple Pendulum System

- 3 Reference Cavity Suspension Commissioning
 - 3.1 Damping and Local Control
 - 3.2 BOSEM Calibration
 - 3.2.1 BOSEM Offset Test
 - 3.2.2 Results
 - 3.2.3 Discussion
 - 3.3 Sensing and Actuation
 - 3.3.1 Derivation of Sensing and Actuation Matrices
 - 3.3.2 Results
 - 3.4 Reference Cavity Suspension Simulation
 - 3.4.1 Transfer Function Simulation
 - 3.4.2 Experimental Procedure
 - 3.4.3 Results
 - 3.5 Reference Cavity Suspension Tests
 - 3.5.1 Transfer Function
 - 3.5.2 Experimental Procedure
 - 3.5.3 Results
 - 3.5.4 Discussion

- 4 Conclusion
 - 4.1 The 10 m Prototype Commissioning, Moving Forward
 - 4.2 Acknowledgments

References

Appendices

A. Simulink Model Parameters

A.1 Script Title: `global_constants.m`

A.2 Script Title: `build_pend.m`

B. Single, Double, and Triple pendulum Calculation

1 Introduction

1.1 Gravitational Waves

In 1916 Albert Einstein, published his Theory of General Relativity, in which he predicted the existence of gravitational waves. The theory states that gravitational waves are formed whenever there is a change in the quadrupole momentum of a given mass distribution, [Einstein'16].

Water waves appear as ripples on the surface of water, gravitational waves are ripples through the fabric of space-time. However the interaction between matter and space time is so small that these waves are incredibly weak. Only enormous astrophysical events can produce gravitational waves with amplitudes where detection is feasible. These events included, supernova bursts, black hole convergence and some binary systems such as neutron star-black holes or two orbiting black holes and so on. There is an advantage to the elusiveness of gravitational waves. The weakly coupled nature of gravitational waves allows them to propagate almost completely unimpaired throughout the whole universe.

Modern astrophysics utilizes electromagnetic radiation and neutrino detection to study the substance of our universe. However there are many astrophysical bodies where such methods of detection are insufficient. Black holes, for example, do not emit light, nor do they emit neutrinos, yet their incredible mass makes them prime targets for gravitational wave observation. There are also regions of space that are obscured from vision such as the center of our own Milky Way galaxy, where interstellar gas obscures the center from view by traditional means. Gravitational waves however, due to their weakly interacting nature, can easily permeate through the whole of our galaxy mostly undeterred. This makes them valuable sources of information about the inner workings of our galaxy and many other, otherwise inaccessible, astrophysical bodies. Gravitational wave astronomy is expected to open a completely new window to the universe and will deeply impact our current perception of it.

1.2 Gravitational Wave Detectors

Detecting Gravitational waves is no small feat. The project is one of the most challenging and ambitious in modern physics. There are two main approaches employed in the detection of gravitational waves, they are; detection via resonant-mass antennas or via laser-interferometers. This paper mainly addresses the later method of detection. The laser-interferometer detection method provides a broad bandwidth of detectable frequencies up to a few kHz of high sensitivity [Goßler'68]. Currently there are 5 interferometric gravitational wave detectors in existence worldwide. These along with some proposed detectors included;

AIGO (Australian International Gravitational Wave Observatory) an Australian detector at Gingin [Ju'04]. This detector has an operating vacuum system with 80 m long arms.

GEO (also known as GEO600), is a German-British project located in Ruthe, Germany [Danzmann'95]. It is based on a Michelson interferometer with arm lengths of 600m, each folded once to obtain an effective length of 1200m.

KAGRA, is a proposed Japanese project. The detector will be located underground in the Kamioka mine in Kamioka-cho, Japan [Somiya,Kentaro'12]. Its subterranean location protects it from a major portion of seismic noise which mostly travels on the surface of the earth's crust. The project is currently planning on installing two interferometers with 3 km long arms.

The **LIGO** (Laser Interferometer Gravitational wave Observatory) collaboration consists of two sites in the US, one in Livingston, Louisiana and the other in Hanford, Washington [Sigg'04]. The two sites both contain Michelson interferometers with 4 km arm lengths.

TAMA (also known as TAMA300), is a Japanese project operating a Michelson interferometer located near Tokyo [Takahashi'04]. The detector has 300m long arms.

Virgo, the French-Italian project is located in Cassia, Italy [Bradashia'90]. It is a Michelson interferometer with 3km arm lengths.

LISA (Laser Interferometer Space Antenna), is the proposed space borne gravitational wave observatory [Vitale'20]. Once realized LISA will consist of three spacecraft arranged in an equilateral triangle with side lengths of roughly $5 \cdot 10^7$ km. It will consist of three coupled interferometers with arm lengths equivalent to the sides of the equilateral triangle.

Most of these detectors are either in development or being upgraded to the next generation of advanced interferometric detectors. Only the GEO detector is currently operating in a more or less continuous observation mode.

1.3 Interferometric Detectors

Though these different projects each implement their own version of the laser interferometer the core of how the instrument works is the same. Most ground based laser interferometers used for gravitational wave detection are, in principle, Michelson interferometers whose mirrors are suspended as pendulums [Torrie'01]. This method of laser interferometry was first done by Forward [Forward'78] and Weiss [Weiss'72] in the 1970's.

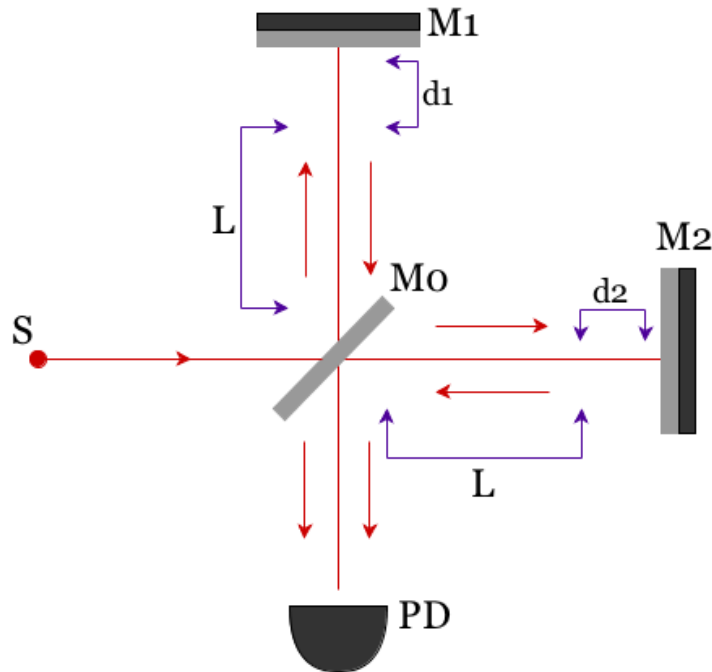


Figure 1 shows a schematic of an interferometer. S stands for the source of the light. M1 and M2 are the two end mirrors of the arms of the interferometer. M0 is the beam splitter. And L is the length of each arm which is the same, save for a small relative motion between the mirrors depicted as d_1 and d_2 . The relative motion can be positive or negative and appears as the sum of the motion in each arm. The light is recombined and detected by the photo detector located at PD.

The image in Figure 1 depicts an outline of a Michelson interferometer. The interferometer has the ability to use light to detect minute changes in distance. It does so by taking advantage of the superposition principle and the properties of coherent laser light. Light from a strong coherent laser is incident on a beam splitter. The light is partially reflected and partially transmitted by the beam splitter into the two arms of the interferometer. Each arm is of length L . The light travels down the length of the arm and reflects off the end mirrors and then back to the beam splitter. The light is then recombined and detected at the photo detector. The pattern of the recombined light will change in intensity as the relative motion of the mirrors varies.

When a gravitational wave passes through the detector the mirrors will distort creating a change in the relative motion between the mirrors, which is internally detected as a change in light intensity at the photo detector. This allows the interferometer to be used to detect gravitational waves directly.

1.4 The 10 m Prototype

In addition to the primary observatories there are additional, smaller scale, interferometric experiments being conducted in the field of gravitational wave research. The 10 m Prototype (see figure 2) located at the Albert Einstein Institute, in Hannover, Germany, is an example of one such project, [Goßler'10]. Though the size of the interferometer limits its ability to detect gravitational waves, new methods and theories can be tested in the smaller 10 m Prototype. The advantage of the 10 m prototype is that it allows for experimentation with new methods and techniques for suspension and optics that might be considered too risky with the larger more delicate observatories.

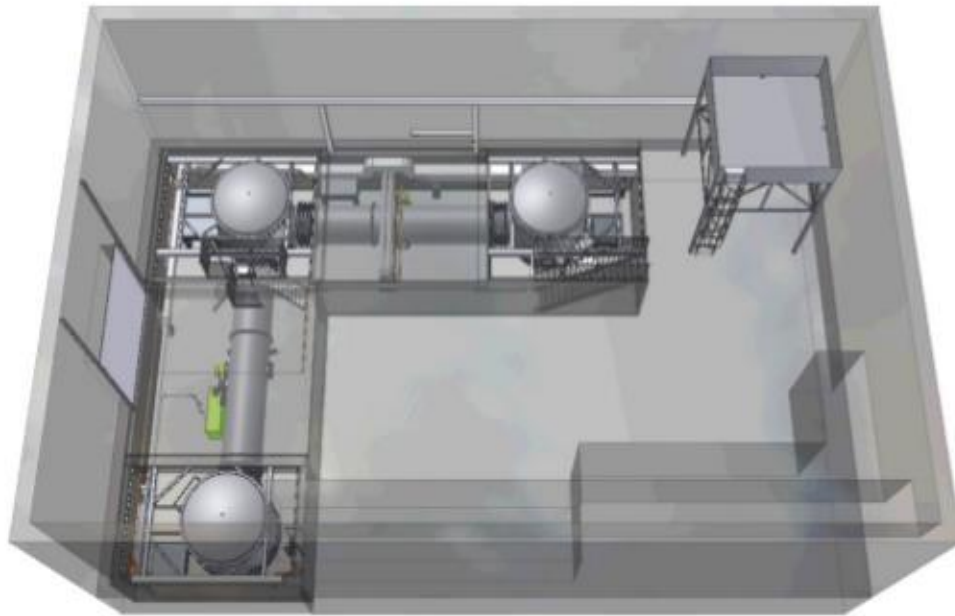


Figure 2 depicts the 10 m prototype which employs a suspension system consisting of seismically isolated tables and multi pendulum suspensions for the test masses. It also utilizes a high vacuum system, [Goßler'10].

The 10 m prototype aims to perform experiments at or below the Standard Quantum Limit (SQL). This would mean that the dominant noise source for the 10 m Prototype would be measurement (shot) noise and back-action (quantum radiation pressure) noise. In order for those noise sources to dominate the interferometer must be well isolated from seismic and thermal noise, by far the two largest sources of external noise limiting the sensitivity of interferometric detectors. In order to reach such sensitivities the 10 m prototype utilizes seismically isolated benches, that will be interferometrically interconnected and stabilized. The interferometer will also be placed within a ultra-high vacuum system. The sensitivity of the 10 m prototype enables it to be used for experiments in the field of macroscopic quantum mechanics.

2 Theory and practice of Optic Suspension

2.1 Noise Sources

The main challenge in detecting gravitational waves is creating a detector sensitive enough to observe the small amplitude signals, gravitational waves produce. The main sources of noise that hinder the sensitivity of ground based laser detectors are;

- Seismic noise, caused by motions of the Earth.
- Thermal Noise, In the mirror test masses and in their suspensions.
- Photon noise.

Seismic noise can result from many naturally occurring phenomena. For example, ocean tides, vehicle traffic near the detectors, and earthquakes, are all regular sources of seismic noise. The test masses of the interferometric gravitational-wave detectors require isolation many orders of magnitude greater than this ground motion. To overcome this detectors employ seismically isolated tables supporting multi pendulum suspension to hold the test masses. This reduces the noise in the detector by many orders of magnitude, [Goßler'68].

Thermal noise is caused by the random motion of the atoms of the test mass mirrors and their suspensions. Sources of thermal noise include; pendulum modes of the suspended test masses, internal modes of the test masses and violin modes of the suspension wires, among others. Modern detectors go to great lengths to minimize thermal noise. In addition to highly sophisticated suspension systems which primarily help isolate the test masses from seismic noise, interferometric detectors are also placed in vacuum systems. Putting the detectors into vacuum reduces the influence of air damping, of refractive index fluctuations and acoustic coupling, as well as helping to reduce thermal noise in the detector, [Goßler'10].

Photon noise, also known as photon shot noise, is caused by the variation of the number of photons hitting the output of the interferometric detector. There is an uncertainty associated with the number of photons detected at the output of the detector. It is this uncertainty that gives rise to shot noise, [Torrie'01]. The sensitivity of an interferometer to shot noise can be improved by increasing the level of input power. However the power of the laser is directly connected to the radiation pressure noise. Radiation pressure noise is caused by the fluctuation of the number of photons reflected off the surface of the test mass. As the laser power increases so does noise due to radiation pressure.

The 10 m prototype aims to characterize Photon noise and Radiation pressure noise. In order to do this the prototype employs a suspension system consisting of seismically isolated tables and multi pendulum suspensions for the test masses. It also utilizes a high vacuum system. This allows the detector to operate with thermal and seismic noise greatly reduced. Leaving Photon noise and radiation pressure noise the dominant sources of noise in the detector, [Goßler'10].

2.2 Optic Suspension and Seismic Isolation

2.2.1 Seismic Attenuation System

The 10 m prototype utilizes three seismically isolated tables placed in three tanks of the vacuum system. It also uses two different types of pendulum suspension to hold the optics of the interferometer. This multi-stage system aims to reduce the seismic motion in the optics below the standard quantum limit.

The first stage of isolation comes from the optical tables. The optical tables are also referred to as the seismic attenuation system, SAS. To reduce differential motion the SAS platforms are inter-linked by a suspension platform interferometer, SPI.

The SAS is a mechanical system on which the optical benches are installed. The system is fully passive, however it is equipped with sensors and actuators for additional feedback control. The design of the SAS is based on the design of the HAM-SAS, [Stochino'09], developed by the aLIGO program.

The SAS provides a large magnitude of isolation. The designed isolation value of the system is 80 dB for vertical and 90 dB for horizontal degrees of freedom. Isolation ranges from very low frequencies of a few hundreds of millihertz to several hundred hertz, [Dahl'12]. Figure 3 shows one of the three optical tables used by the 10 m prototype.

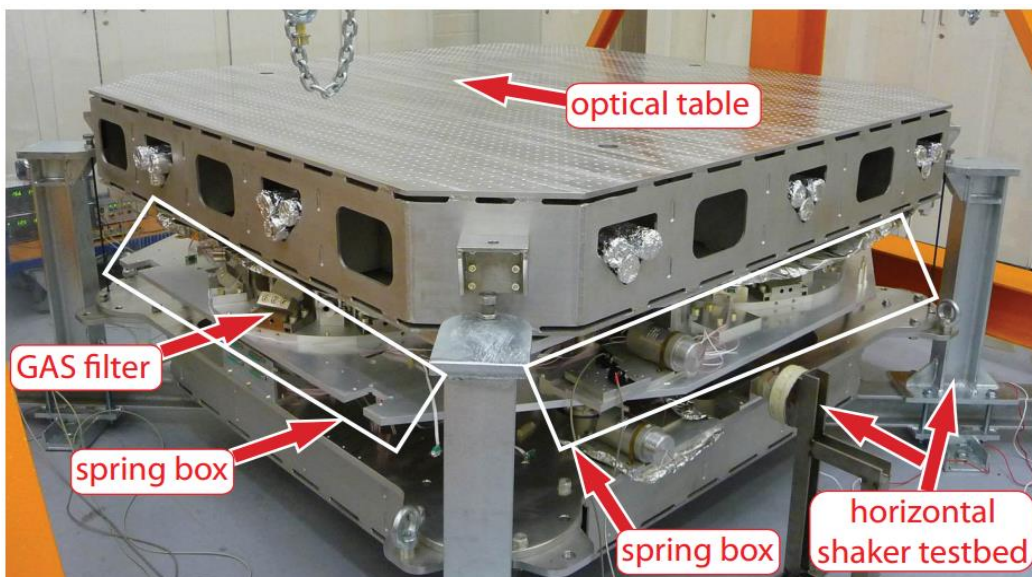


Figure 3 is a photograph of a fully assembled AEI SAS outside of the vacuum system. The weight is about 1800 kg and the dimensions of the optical bench are 1.75m×1.75m, [Dahl'12].

2.2.2 Optic Suspension

The final stage of isolation is provided by the mirror suspensions. There are three different types of suspension utilized by the 10 m prototype. They are;

- Steering mirror suspensions
- Reference cavity mirror suspensions and
- The SQL interferometer mirror suspension.

The steering mirror suspension is a one stage pendulum hung from steel wires. The steering mirrors are used to steer the beam and thus have active control and damping.

The reference cavity mirror suspension provides a higher degree of seismic isolation than that of the steering mirrors. The mirrors will be suspended by a three stage pendulum system. The reference cavity also utilizes cantilever springs, at the upper most mass and at the point of attachment to the suspension cage, see Figure 4. These cantilever springs provide vertical isolation while the pendulum provides horizontal isolation. The suspension utilizes steel wires. Local control of the mirrors and damping of the Eigen modes is done at the upper mass, [Dahl'12]. Section 3 of this paper will focus on the modeling and local control of the reference cavity suspension.

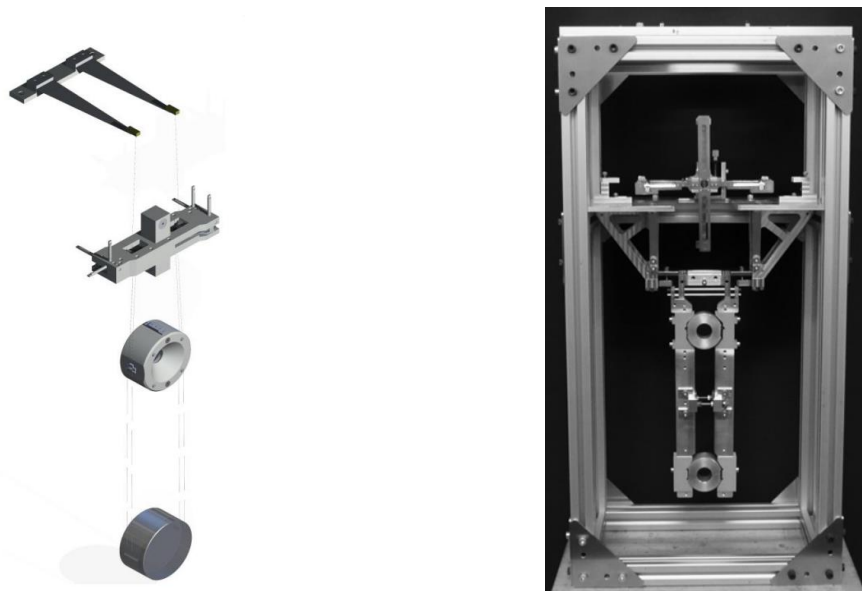


Figure 4, the image on the left depicts the core of the Reference Cavity Suspension without the surrounding suspension cage. It consists of three horizontal stages (pendulum), and two vertical stages (cantilever springs), [Westphal'11]. The image on the right is a picture of one of the suspensions for a single mirror in the 10 m prototype, [Cumming'12].

The SQL interferometer mirror suspension is very similar to that of the Reference cavity suspension. It utilizes a triple pendulum suspension as well as cantilever springs at the point of attachment to the suspension and at the upper most mass. Steel wires will be used to hang the

upper and intermediate masses. The final mass will be hung from four fused silica wires. The fused silica final stage lowers the suspensions thermal noise. Damping will be applied at the upper most mass as well as weekly at the test mass.

2.3 Mathematical Modeling of Single and Triple pendulum Suspensions

2.3.1 Introduction and Parameters

In order to control the position of the tests masses it is important to model the motion of the pendulum suspension. The suspension of the 10 m prototype utilizes triple pendulum suspension systems. To begin we will describe the behavior of a single pendulum and then generalize to the triple pendulum case. The mathematical derivation can become quite complex. Thus an abbreviated derivation is given for the vertical degree of freedom as well as the couple pitch and longitudinal degrees of freedom. All other degrees of freedom are described briefly with limited mathematical derivations. For more rigorous derivation for the equations of motion of a single and triple pendulum see the thesis, Development of Suspension for the GEO 600 Gravitational Wave Detector, written by Dr. Calum Torrie [Torrie'01].

A single pendulum is shown in Figure 6 below. In modeling this pendulum we considered the effects of gravity, the stretching of the wires and the geometrical properties of the system. Other characteristics of the system include negligible damping and that the wires act as linear springs obeying Hooke's law. The mass is also assumed to be rigid.

A single pendulum has six degrees of freedom, three translational, and three rotational. The degrees of freedom are as follows;

- Longitudinal, translational motion parallel to the X-axis.
- Side, translational motion parallel to the Y-axis.
- Vertical, translational motion parallel to the Z-axis.
- Roll, rotation about the X-axis.
- Pitch, rotation about the Y-axis.
- Yaw, rotation about the Z-axis.

They are also displayed in Figure 5 for a rigid rectangular mass, [Westphal'13].

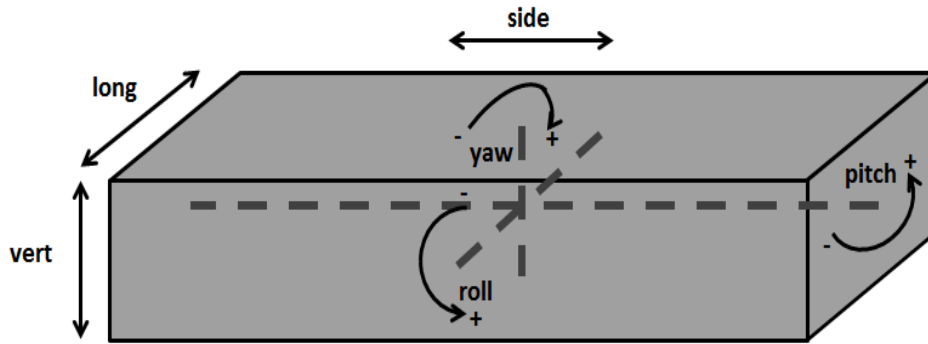


Figure 5 depicts the degrees of freedom as they relate to a rigid rectangular mass. The upper mass of the suspensions of the 10 m prototype utilize rectangular masses connected by two wires to the suspension [Westphal'13].

Using Newton's second law, we can write down the differential equations of motion for the single pendulum system. To do this we use the following parameters;

- s = half the separation of the wires
- l = the length of the wire,
- $t1$ = the half separation of the wires in the Y direction at the suspension point
- $t2$ = the half separation of the wires in the Y direction at the mass
- d = the distance the wires break-off above the line through the centre of mass
- k = the spring constant of one wire

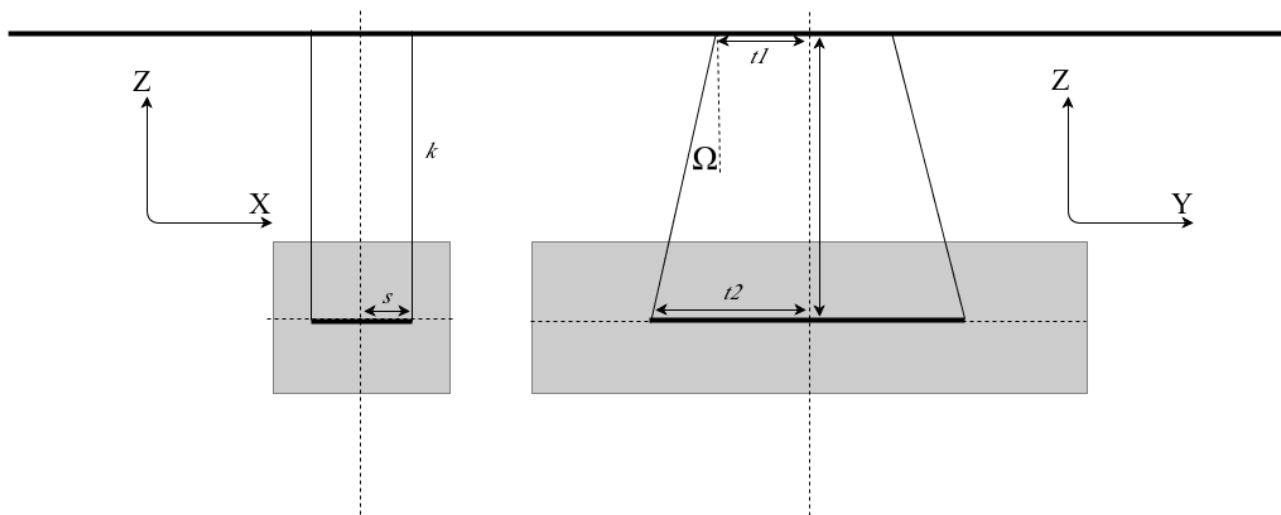


Figure 6 depicts a rectangular mass suspended by four wires. The length of the wires is l , the angle of attachment with respect to the vertical is Ω , half the separation of the wires at the point of attachment to the suspension along the Y-axis is $t1$, half the separation of the wires at the point of attachment to the mass along the Y-axis is $t2$, and half the separation of the wires at the point of attachment to the mass along the X-axis is s .

The differential equations of motion are dependent on the degrees of freedom. Some degrees of freedom are independent to first order and are uncoupled from the others. This is the case for Vertical motion. Others, such as Longitudinal which is coupled with pitch, must be described with the same set of coupled differential equations.

2.3.2 Vertical

The upper mass of the 10 m prototype can be described as a single pendulum, with mass m , connected by two wires of length l and spring constant k . The wires are at an angle, Ω , with the vertical. The tension in the wires is described by the following equation, where Δl_0 is the change in length from the unstretched string length, l_0 , to the suspended equilibrium length, l ;

$$T = \frac{mg}{2\cos\Omega} = k \Delta l_0 \quad (2.1)$$

The right hand side of figure 4 depicts the system in static equilibrium, with the mass hanging from the wires.

A force applies a downward offset to the mass by a small amount z from the equilibrium position. The length of the wires and their angle from vertical are changed to l' and Ω' . Tension in the wire is also changed due to gravitational loading. The new tension in the wires is described by the following equation;

$$T' = \frac{mg}{2\cos\Omega'} = k \Delta l_0' \quad (2.2)$$

The motion of the system can be described by implementing Newton's second law and Hooke's law. Since the wires can be described as springs we can make the following statements.

By Newton's second Law

$$mz'' = F. \quad (2.3)$$

By Hooke's law

$$F = k \Delta l. \quad (2.4)$$

thus

$$mz'' = k \Delta l. \quad (2.5)$$

Where Δl is the change in the length of the wires. Using the initial tension and the tension after the offset we can deduce the change in length of the wires and thus describe their motion. This work has been done out in great detail in the thesis of Dr. Calum Torrie, [Torrie'01], the detailed calculation are shown there. From his work it is found that,

$$\Delta l = z \cos\Omega + \frac{mg}{2k} \left(\frac{z \tan^2 \Omega}{1} \right). \quad (2.6)$$

Thus the equation of motion in the vertical direction is

$$mz'' = -\left(sk\cos^2\Omega + \frac{mg\sin^2\Omega}{l\cos\Omega} \right)z. \quad (2.7)$$

The above equation models simple harmonic motion. Due to this we can deduce that the vertical frequency of a single pendulum is;

$$f_{\text{vertical}} = \frac{1}{2\pi} \sqrt{\left(+\frac{2k\cos^2\Omega}{m} + \frac{g\sin^2\Omega}{l\cos\Omega} \right)}. \quad (2.8)$$

These equations describe a single pendulum with two wires. For the case of 4 wires you replace the k with $2k$ in equation (2.7).

2.3.3 Pitch and Longitudinal

Consider a single pendulum with two wires. Rotate the mass by an angle ϕ to the vertical, along the X-axis. This rotation also causes a displacement along the X-axis. Let the length of the wires be l and the angle of the wires from vertical be θ . The angle ϕ is defined by the rotation of the centre of mass. The displacement x_n is the motion of the centre of mass from its initial equilibrium position. The displacement x_0 is the linear displacement of the wires at the point of attachment to the suspension. Both displacements x_n and x_0 are along the X-axis. In this example the attachment points of the wires to the mass are along the axis of the centre of mass. Figure 7 displays these features.

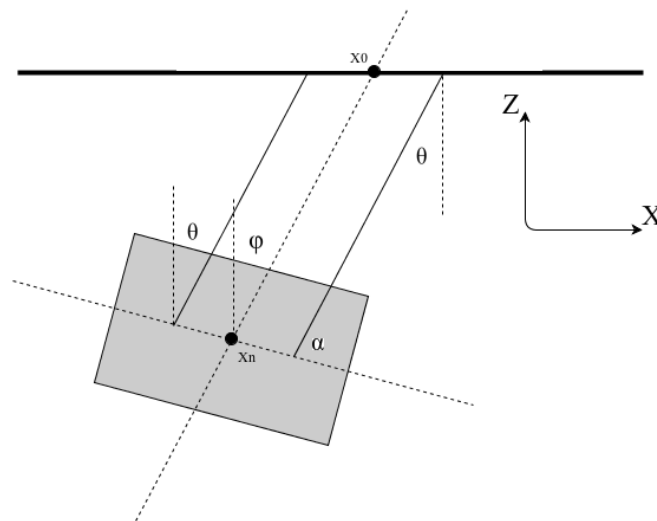


Figure 7 depicts a rectangular mass suspended by two wires of length l and spring constant k . The mass is rotated and angle ϕ with respect to the vertical along the X-axis. The angle of the wires with respect to the vertical is θ and the angle of the wires with respect to the axis of the centre of mass is α . The

displacement x_n is the motion of the centre of mass from it's initial equilibrium position. The displacement x_0 is the linear displacement of the wires at the point of attachment to the suspension.

For small angles we can use the following approximation to find the values of ϕ and θ ;

$$\phi = \sin\phi = \frac{x_n - x_0}{l} \quad (2.9)$$

$$\text{and } \theta = \sin\theta = \frac{x_n - x_0}{l}. \quad (2.10)$$

In the case where the attachment points of the wires to the mass are along the axis of the centre of mass these angles will be equal. However if the attachment point were higher or lower this would not be the case. It is also assumed that both wires are of the same length l .

The mass tilts due to a component of the restoring force caused by the tension in the wires. For one of the wires the component of the restoring force is $T_2 \sin(\phi - \theta + \alpha)$ and for the other wire is $T_1 \sin(\alpha - \phi + \theta)$. Since ϕ and θ are equal it simplifies to $T_1 \sin(\alpha)$ and $T_2 \sin(\alpha)$. The values T_1 and T_2 are the tension in each wires and are equivalent to;

$$T_1 = \frac{mg}{2} + k\Delta l \quad (2.11)$$

$$\text{and } T_2 = \frac{mg}{2} - k\Delta l. \quad (2.12)$$

The value Δl is the change in the vertical height as the mass tilts. The equation of motion for the two wires will depend on the Torque which is equal to the distance crossed with the perpendicular component of the force. This fact gives us the following equation of motion for the tilt for a two wire suspension;

$$I_y \phi'' = -sT_1 \sin(-\alpha) - sT_2 \sin(\alpha). \quad (2.13)$$

Here I_y is the moment of inertia about the Y-axis. Carrying out a few substitutions we can simplify the above equation. Making a small angle approximation and utilizing that for small distances $\Delta l = z = s\phi$, where s is half the separation of the wires at the point of attachment to the mass and ϕ is a small angle. We get the following equation;

$$I_y \phi'' = -2ks^2 \phi \quad (2.14)$$

where $\cos(\alpha) = 0$ and $\sin(\alpha) = 1$.

The longitudinal equation of motion is

$$mx_n'' = -mg\theta. \quad (2.15)$$

Since θ is equivalent to ϕ we can exchange them to get the following;

$$mx_n'' = -mg\phi. \quad (2.16)$$

Thus from equations (2.14) and (2.16) show that pitch and longitudinal motion are coupled.

In the case where the point of suspension is not aligned with the centre of mass the final equations are not quite the same. If the wires are attached a distance d above the center of mass along the Z-axis the equations are as follows;

$$I_y\phi'' = \frac{mgd}{l}(x_n - x_0) + (-mgd - \frac{mgd^2}{l} - 2ks^2)\phi \quad (2.17)$$

and
$$mx_n'' = -\frac{mg}{l}(x_n - x_0) + \frac{mgd}{l}\phi. \quad (2.18)$$

These equations are derived in the thesis of Dr. Calum Torrie [Torrie'01]. Again it is demonstrated that the pitch and longitudinal degrees of freedom are coupled.

2.3.4 Yaw

For the purpose of this paper the equations of motion for the remaining degrees of freedom, will simply be stated below. It should be known that the derivations are similar to the ones shown above for Vertical, Pitch and Longitudinal.

In the case of a single pendulum with two wires the Yaw degree of freedom is not coupled to any other degree of freedom. Let the mass of the pendulum be m and the rotation about the Z-axis be given by the angle σ . The variable t is the distance the wire is from the vertical line through the centre of mass, this is equivalent to t_1 and t_2 shown in Figure 6 if t_1 and t_2 were equal. The equation of motion below is true in the case where the wires are attached along the axis of the centre of mass;

$$I_z\sigma'' = -\frac{mgt^2}{l}\sigma. \quad (2.19)$$

This result varies if the wires are attached to the suspension at an angle Ω as depicted in Figure 4. In this case the equation of motion for a single pendulum, hung from two wires is as follows;

$$I_z\sigma'' = -\frac{mgt_1t_2}{l\cos\Omega}\sigma. \quad (2.20)$$

The derivation of these equations and other pendulum models can be found in the thesis of Dr. Calum Torrie, [Torrie'01].

2.3.5 Sideways and Roll

Sideways and roll motion are derived in a similar manner as longitudinal and pitch. Just as is the case with longitudinal and pitch, the sideways and roll degrees of freedom are coupled. These degrees of freedom become even more strongly coupled when the wires are angled along the Y-axis or the attachment points of the wires to the mass are not along the axis of the centre of mass.

Consider the case where the mass is suspended by two wires sloping at an angle Ω to the Z-axis, as seen in Figure 6. Where variables t_1 , t_2 and d are defined above in section 2.3.1. Let the mass be displaced a distance $\Delta y = y_n - y_0$ and rotated an angle Ψ to the vertical, along the Y-axis. The equation of motion for such a system is given by the following coupled equations;

$$\begin{aligned}
 m y_n'' &= \left(-\frac{mg \cos \Omega}{l} - 2k \sin^2 \Omega \right) (y_n - y_0) \\
 &- \left(+\frac{mg d \cos \Omega}{l} - \frac{m g t_2 \sin \Omega}{l} + 2k d \sin^2 \Omega + 2k t_2 \sin \Omega \cos \Omega \right) \Psi
 \end{aligned}
 \tag{2.21}$$

and

$$\begin{aligned}
 I_x \Psi'' &= \left(+\frac{m g t_2 \sin \Omega}{\cos \Omega} - m g d + \frac{2 m g d t_2 \sin \Omega}{l} - \frac{m g d^2 \cos \Omega}{l} - \frac{m g t_2^2 \sin^2 \Omega}{l \cos \Omega} \right) \Psi \\
 &+ \left(-4 k d t_2 \sin \Omega \cos \Omega - 2 k d^2 \sin^2 \Omega - 2 k t_2^2 \cos^2 \Omega \right) \Psi \\
 &+ \left(+\frac{m g d \cos \Omega}{l} - \frac{m g t_2 \sin \Omega}{l} + 2 k d \sin^2 \Omega + 2 k d t_2 \sin \Omega \cos \Omega \right) (y_n - y_0)
 \end{aligned}
 \tag{2.22}$$

For the case with four wires the k in these equations would become $2k$, where k is the spring constant of one of the wires. For further derivation of these equations and other pendulum models refer to the thesis of Dr. Calum Torrie, [Torrie'01].

2.3.6 Triple Pendulum System

The goal of the triple pendulum suspension systems employed in ground based interferometers is to isolate the detector from ground motion. The triple pendulum suspension does so by taking advantage of intrinsic properties that pendulum systems poses, and exploiting them in order to reduce motion at desired frequencies.

A pendulum is a simple harmonic oscillator. As such it possesses a resonant frequency where when driven at this frequency the amplitude of the motion of the pendulum will increase dramatically. This driving force, in the case of test masses in an interferometer, can be seismic vibrations. However if the pendulum is driven above resonance the increase in the motion of the

pendulum decreases by a factor of one over the frequency squared, for a single pendulum. It is this quality that is exploited to reduce the seismic noise in pendulum suspensions.

For a single pendulum each degree of freedom has a resonant frequency and associated Eigen mode. The resonant frequencies for a single ideal pendulum, with length l , in the longitudinal degree of freedom is as follows;

$$f = \frac{1}{2\pi} \sqrt{\frac{mg}{l}} \quad (2.23)$$

In the case of a triple pendulum suspensions you gain an additional resonances for each pendulum, per degree of freedom. A triple pendulum has 18 resonants, three for each degree of freedom. Figure 8 shows an example of the extrema of position for the three Eigen modes of the longitudinal degree of freedom. The masses and wire lengths reflect those of the reference cavity suspension in the 10 m prototype.

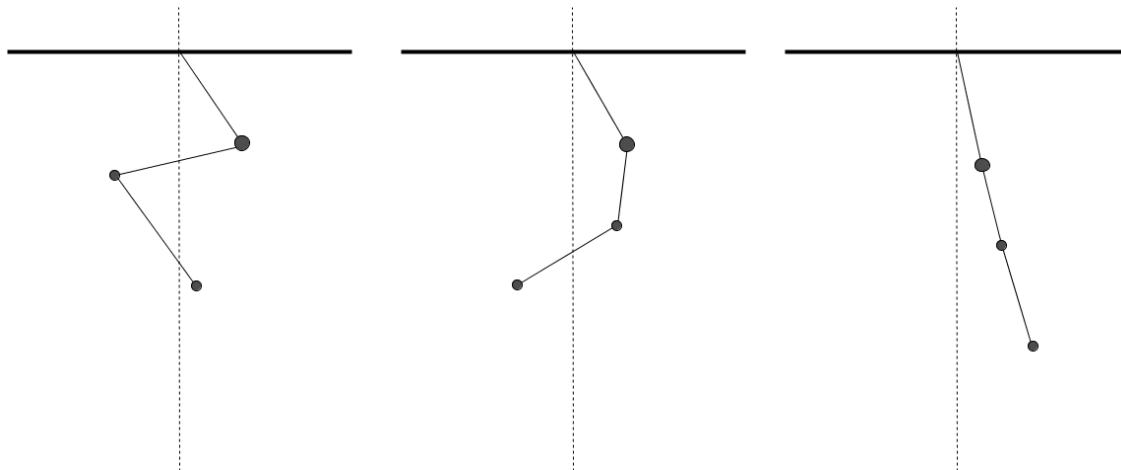


Figure 8 depicts the longitudinal modes of a triple pendulum. The masses, from top to bottom, are 1050g, 950g and 850 g. The length of the wires are, from top to bottom, 0.22m 0.20m and 0.35m. These are the wire lengths and masses of the reference cavity suspension for the 10 m prototype. The key difference is that the 10 m prototype suspension utilizes 2 wires, 4 wires and 4 wires, from top to bottom. For the longitudinal degree of freedom the above modes are a good approximation.

The triple pendulum system gains new resonants and thus less sensitivity at and around those frequencies. However it achieves further noise reduction below these resonants. For each pendulum you gain a factor of one over the frequency squared, leaving a power of six noise reduction below resonants. The resonant frequencies for the longitudinal degree of freedom of a triple pendulum, as seen in Figure 8, are as follows.

$$\begin{aligned} f_1 &= 1.827 \text{ Hz} \\ f_2 &= 1.125 \text{ Hz} \\ f_3 &= 0.485 \text{ Hz} \end{aligned}$$

The calculations for the resonance of a single and triple ideal pendulum system can be found in appendix B.

The ideal case provides the logical defense of this method of isolation. In order to employ this as a practical technique in ground based interferometric detectors, more robust models of the system are made. The pendulum suspensions is designed in such a way that the resonance of the system are below the range of detected frequencies. Sections 2.3.1 through 2.3.5 demonstrate the necessary calculations and equations for the single pendulum case. These calculations are generalize to model a triple pendulum system in the thesis of Dr Calum Torrie, [Torrie'01]. The equations of motion are not addressed in more detail in this paper but are employed in computer simulations which produce transfer functions and other figures for the Reference Cavity suspension of the 10 m prototype. Appendix A states the parameters and properties used in the calculation of these functions and resonants.

A mathematical model for a triple pendulum system allows one to predict the motion of the system. This modeling is then utilized in the local controls of the suspension system in the form of position and velocity damping. It is particularly important for suspensions that utilize control at the upper most mass and not at the test mass itself. The goal of the suspension is to reduce motion in the test mass. In particular, in the degrees of freedom that affect the path of the light incident upon the mirrors most strongly, such as longitudinal motion. Sensors and actuators are located at the upper most mass. However it is the motion of the test mass itself that must be controlled. Thus the position of the test mass is controlled based on the motion and position of the upper most mass, using the equations of motion for the system.

3 Reference Cavity Suspension Commissioning

3.1 Damping and Local Control

Damping and Local control is provided for the upper mass of the Reference Cavity Suspension. The local control is active in all six degrees of freedom. Active damping at the upper mass ensures that the test mass is isolated from the local control noise by the double pendulum below. The damping system uses six BOSEMs (Birmingham Optical Sensor and Electro-Magnetic actuator). Figure 9 depicts the location of the six BOSEMs, A,B,C,D,E,F, on the upper mass of the reference cavity.

The BOSEM is a collocated sensor and actuator. The motion of the suspended mass is sensed by the BOSEM, whose signal is filtered, amplified and sent to the main digital control system. The signal is then processed, optimized and feedback through the coil-driver amplifier to the BOSEM coils. This actuates the suspended mass. The BOSEM senses the position of a flag which is attached to the upper mass via a magnet. The BOSEM itself does not come in contact with the suspended masses. In order to actuate on the masses, current is run through a coil in the BOSEM. This current applies a force to magnet which is glued to the base of the flag, thus moving the mass.

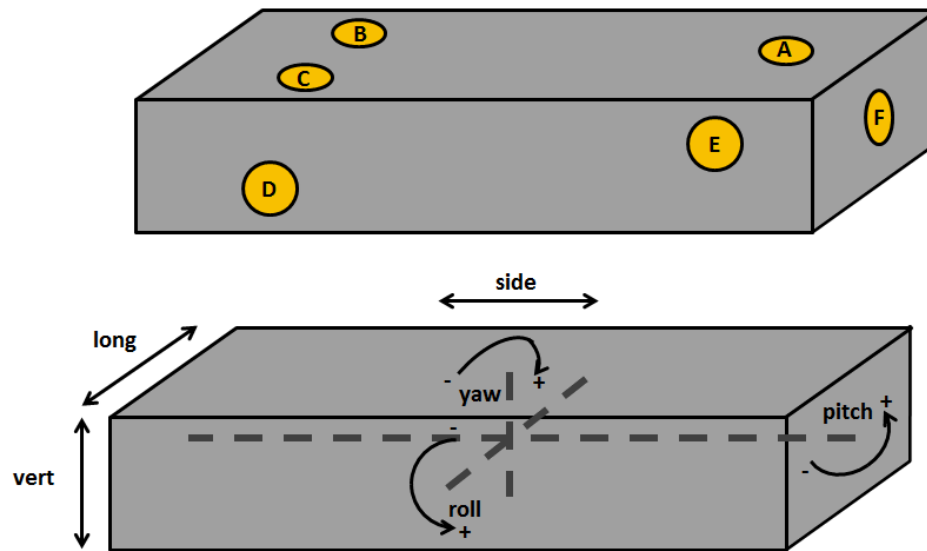


Figure 9 depicts the location of the six BOSEMS A,B,C,D,E,F on the upper mass of the Reference Cavity suspension as well as the degrees of freedom for reference, [Westphal'13].

The placement of the BOSEMS is designed such that, a particular sets of BOSEMS can sense and actuate on individual degrees of freedom. Damping and control of the longitudinal and yaw degrees of freedom are provided by BOSEMS D and E. Damping and control of the vertical degree of freedom is provided by BOSEMS A,B,C. Damping and control of side and roll

degrees of freedom is done by the F BOSEM. Damping and control of the pitch degree of freedom is done using BOSEMs B and C.

Careful modeling and tests must be conducted so that damping is optimized for the spacing of the coils, as seen in Figure 9. In the next few sections the optimization of the Reference Cavity suspension will be described.

3.2 BOSEM Calibration

3.2.1 BOSEM Offset Test

In order to properly calibrate the BOSEMs a test of the independence of their sensing and actuation was conducted. The goal was to determine if there was any issue with the individual BOSEMs, as well as to test for any sort of cross coupling between BOSEMs. This also allows for testing of the separation of the degrees of freedom in actuation and sensing.

The test consisted of applying a force or a momentum to each of the coils of the BOSEMs respectively and measuring the resulting displacement sensing from each BOSEM. A null measurement was taken at the beginning and end of the test as well as several times intermediately. It should be noted that some coils required more or less force depending on their sensitivity. The force applied to each BOSEM during the course of the test is listed below, in the order they were applied. Care was taken to ensure that the force applied did not cause the mass to move out of the sensing range of the BOSEMs.

After applying a force the position of the flag for each BOSEM was measured and noted. Measurements were taken as quickly as possible, to allow for less drift in the suspension. Measurements were taken for every state of excitation. They were also taken before, twice during and after the test, where there was no actuation on any of the BOSEMs, this provided the null measurement.

3.2.2 Results

Individual excitations of BOSEMs were plotted versus the sensing in each BOSEM. The results were centered about the null measurement. The actuation of the BOSEMs was also transformed to describe the equivalent actuation on degrees of freedom. Plots of this are shown below.

The sequential actuation on each BOSEM A-F, and the response to that actuation from the rest of the BOSEMs, is depicted in Figure 10. Damping was applied during this test. The offsets applied in order are A at 3mN, B at 3mN, C at 3mN, D at 1mN, E at 1mN, F at 20mN.

The sequential actuation on each BOSEM A-F, and the response to that actuation in the degrees of freedom, is depicted in Figure 11. Damping was applied during this test. The offsets applied in order are A at 3mN, B at 3mN, C at 3mN, D at 1mN, E at 1mN, F at 20mN.

The sequential actuation in multiple BOSEMs, and the response to that actuation from the rest of the BOSEMs, is depicted in Figure 12. Damping was applied during this test. The offsets applied in order are D and E at 10mN , B at 3mN and C at -3mN, B and C at 1.5mN, A at 3mN with B and C at 1.5mN, D at .4mN and E at -.4mN. The combination of BOSEM actuations have the geometric properties of also actuating on individual degrees of freedom. They have the following relationships;

- $(D+E)/2$ corresponds to a motion in the Long dof.
- $(B-C)/2$ corresponds to a motion in the Pitch dof.
- $(B+C)/2$ should be equal to A and correspond to a motion in the Roll dof.
- $(A+(B+C)/2)/2$ corresponds to a motion in the Vert dof.
- $(D-E)/2$ corresponds to a motion in the Yaw dof.

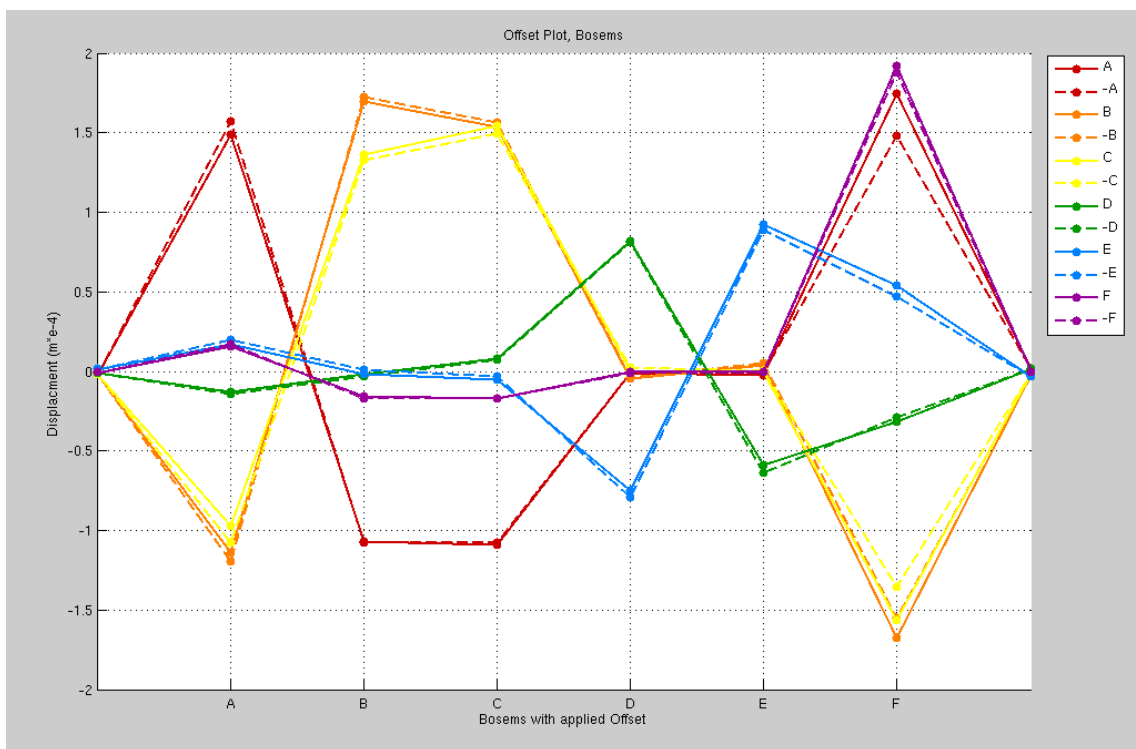


Figure 10 depicts the sequential actuation on each BOSEM A-F and the response to that actuation from the rest of the BOSEMs.

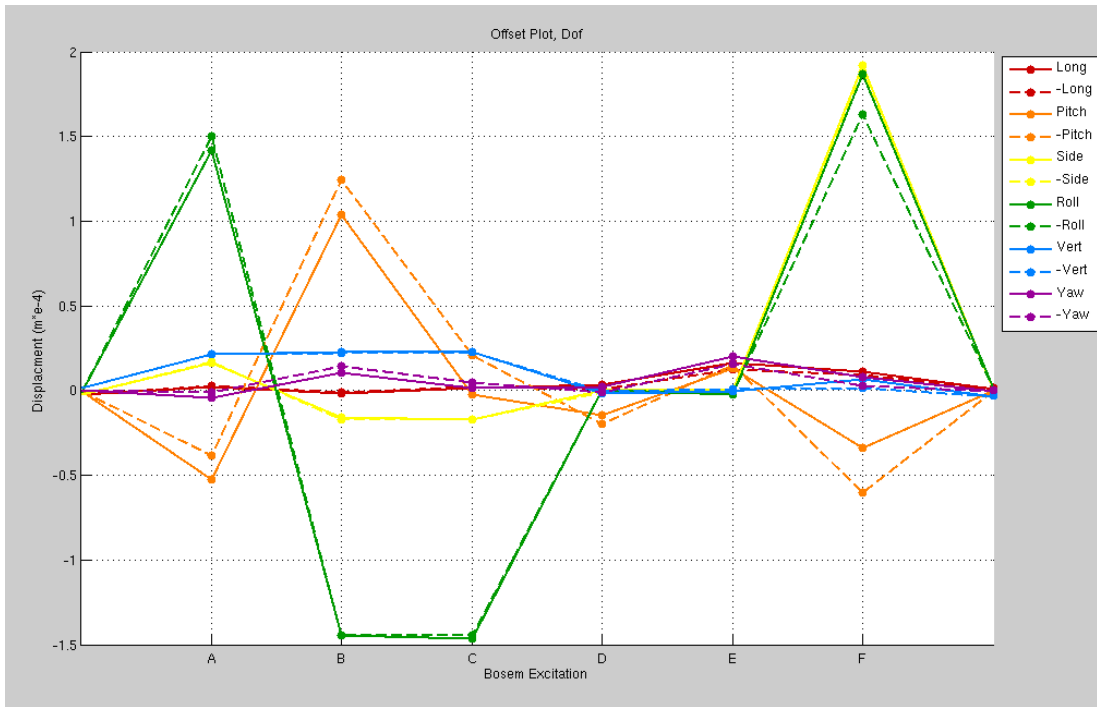


Figure 11 depicts the sequential actuation on each BOSEM A-F and the response to that actuation in the degrees of freedom.

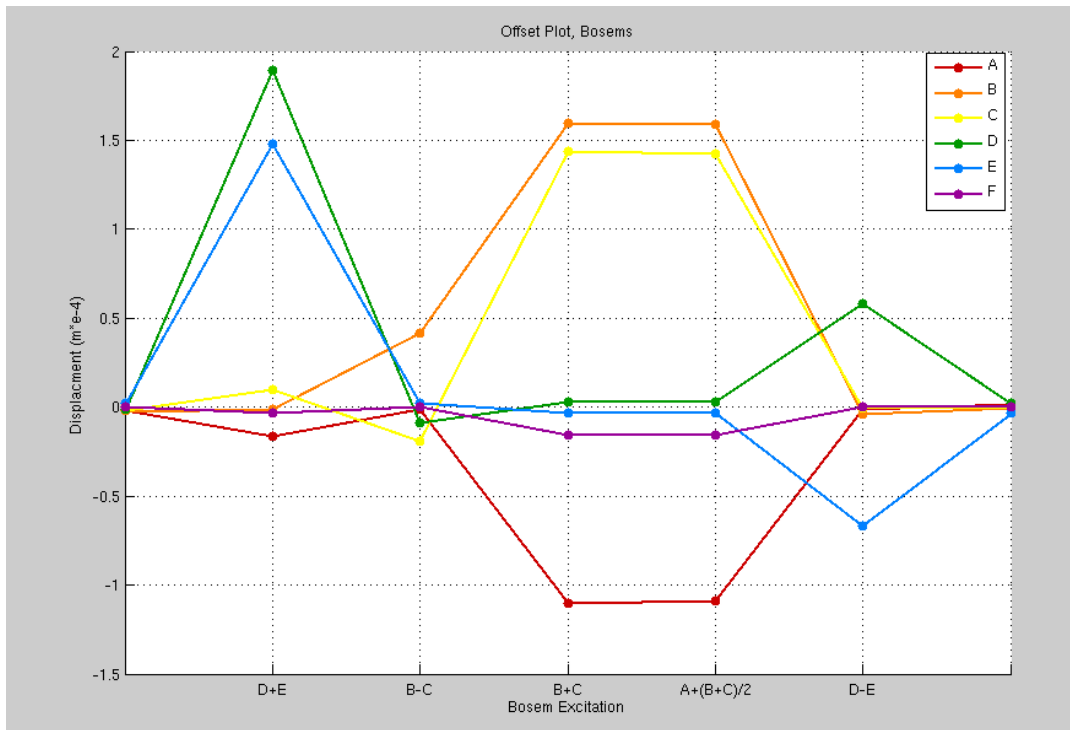


Figure 12 depicts the sequential actuation in multiple BOSEMs and the response to that actuation from the rest of the BOSEMs.

3.2.3 Discussion

Much information can be interpreted from figures 10-12. To begin there are some obvious non-symmetries in figure 10 which become more apparent in figure 11, the degree of freedom separation. One of the first most glaring unexpected results can be seen in Figure 11. An actuation in C does not cause motion in pitch, while an actuation in B does. This is contrary to the expected and desired result of an equal and opposite motion in pitch due to equivalent actuations in C and B.

This could be due to insufficient gain in the C sensor. Increasing the gain by about 1.1-1.2 times its current value would be sufficient to match values seen in the B sensors. This explanation is also supported by the fact that the C-BOSEM had the most varying open light voltage. Although during the calibration $\sim 1/20,000$ meters per volt was corrected by the open light voltages of the BOSEM, this might explain the difference. Adding more gain to C would better match B&C when acting on A, as well as when acting on F. Furthermore the effect from B-actuation onto the C-readout would match the effect of C-actuation onto B-readout. In other words; B and C-actuation would cause opposite pitch in Figure 11. Also an F-actuation would cause no pitch. It could also be the case that D needs more gain. Properly increasing the gain on D would mean that D and E would cause the same long-movement.

Another issue uncovered in this test is that an F-actuation (sideways) causes a large amount of motion in Yaw. It is unlikely that this is caused by a misplacement of the magnet as compared with D & E-actuation (90mm lever arm) the misplacement of the magnet should be less than a few mm (ratio: one to tens). However the pendulum reacts with about half the yaw movement which cannot be corrected by adjusting gains. This finding provides the first hint for magnetic cross coupling.

Looking back to Figure 9 we can see that magnet E (long & yaw) is quite close to coil A (roll,vert) and F (side). The same is true for magnet D being close to coil C. The idea of magnetic cross coupling is supported by the following observations from Figure 10.

- A has more influence on E than on D.
- C has more influence on D than on E.
- B has much less influence on D than C has.
- F has more influence on E than on D.

There is potential for the F (side) actuation to couple to roll in the following three ways:

- First the uppermost wires are not parallel. In that case the suspension would roll around the intersection point of the wires.
- Second pushing the mass to the side moves the center of mass. This loads one blade (the one at the side you are pushing to) more, which then bends down more. This is causing some rolling around a point below the upper mass. Therefore the first effect is compensated (partly).

- Third a magnetic field in coil F acts on the A-magnet. Pushing F results in pushing A causing roll (around a point above the upper mass).

Furthermore pushing on F doesn't cause exactly the opposite of pulling. This can be seen by comparing the solid and dashed lines in Figure 11. In particular the influence onto roll and yaw are different. This may mean, the movement of the upper mass with the magnets on is already so big, that the magnets are experiencing different magnetic field gradients (forces) or different directions of field line (torques).

To verify whether or not the problem was due to the magnetic cross coupling theory one final test was conducted. Magnet D was removed and replaced by an aluminum spacer of the same thickness (glued with quick drying super glue, Sekundenkleber). Currents were applied to coils B and C. After doing so it could be seen that the long reaction was almost completely gone, but yet a small amount of yaw motion still remained! Roll still induced sideways motion at sensor F.

There are steps that can be taken to further investigate this phenomenon and potentially correct it. The first step would be to better characterize the shadow sensor gains. There may be some combinations of gains that can be weighed against each other without having to rely on either the corrected actuation strength or the corrected shadow sensor calibrations. Another possible solution would be to build a new actuation matrix which takes into account magnetic crosstalk. The goal of this new matrix would be to calibrate all actuators so that individual degrees of freedom can be acted on and magnetic cross couplings can be eliminated.

3.3 Sensing and Actuation

3.3.1 Derivation of Sensing and Actuation Matrices

The upper mass of the suspension of the Reference cavity is sensed and controlled using BOSEMs. The placement of these BOSEMs is depicted in Figure 9. In order to utilize the BOSEMs the sensing input must be interpreted and translated into an actuation output. To do this sensing and actuation matrices are derived. The sensing matrix converts the sensor signals into the optic's positions and orientation. The actuation matrix converts these position signals into actuator output signals. The optic's position is referenced to its Eigen modes.

To determine the sensing and actuation matrices one calculates the relation between the sensing and actuation in the BOSEM basis to that of the degree of freedom basis. The calculation follows from the geometry of the upper mass.

The first image in Figure 9 depicts the location of the six BOSEMs on the upper mass. The second image shows the axes; side, long and vert about which the three rotational degrees of freedom roll, pitch and yaw rotate. BOSEMs C and B are displaced +/- 16 mm from

the side axis. BOSEMs E and D are displaced +/- 90 mm from the vert axis and +/-11 mm from the side axis.

The geometry of the system makes it easier to imagine the relation between position and the degrees of freedom, so first the matrix that takes the degree of freedom position and converts that to the BOSEM sensed position is inferred. The matrix has columns (Long, Pitch, Side, Roll, Vert, Yaw) and rows (A, B, C, D, E, F). The units of Long, Pitch and Side are meters, while Pitch, Roll and Yaw are in radians per meter.

Imagine the upper mass is displaced in the Long degree of freedom, if there is only motion in long you would expect to sense this equally in the D and E BOSEMs and to see no change in the other BOSEMs. This is represented in the first column of the sensing matrix that takes degrees of freedom to BOSEMs shown below. The second column represents a motion in the Pitch degree of freedom. If the mass only rotates in pitch you would expect to see this in BOSEMs B,C,D and E. The amount of displacement sensed in B should be equal and opposite of that sensed in C. The same is true in the case for the D and E BOSEMs. The amount of motion is proportional to the lever arm of the rotation. The distance from the side axis of B and C is 16 mm thus the sensing in B and C are plus and minus 0.016m. The derivation of the other columns is done using the same reasoning utilized to derive Long and Pitch. The full matrix that takes the sensed position of the BOSEMs and converts that to the Degree of freedom basis is shown below.

Sensing_DOFtoBOSEM =

$$\begin{pmatrix} 0 & 0 & 0 & 0.09 & 1 & 0 \\ 0 & 0.016 & 0 & -0.09 & 1 & 0 \\ 0 & -0.016 & 0 & -0.09 & 1 & 0 \\ 1 & -0.011 & 0 & 0 & 0 & 0.09 \\ 1 & 0.011 & 0 & 0 & 0 & -0.09 \\ 0 & 0 & 1 & 0 & 0 & 0 \end{pmatrix}$$

The above matrix is then inverted to find the sensing matrix, which takes BOSEM sensing to degree of freedom sensing.

To derive the Actuation matrix a similar approach is taken. Due to the geometry of the system it's easier to start with an actuation in the BOSEMs and then infer what the resulting motion would be in the degrees of freedom. This matrix will be the inverse of the actuation matrix. The matrix has columns (A, B, C, D, E, F) and rows (Long, Pitch, Side, Roll, Vert, Yaw).

Imagine the upper mass is actuated on with equal force and direction with the D and E BOSEMs. Due to the geometry of the upper mass and the location of the BOSEMs you would expect motion in only the longitudinal degree of freedom. Thus the first row, which corresponds to an actuation in Long, has 1's in the D and E columns. The sixth row corresponds to an actuation only in the Yaw degree of freedom. If you actuated on D and E equally and oppositely

you would expect the mass to rotate in the Yaw degree of freedom. The magnitude of this actuation is multiplied by the lever arm of the force applied. The lever arm of the D and E BOSEMs about the vertical axis is 0.09 m. The derivation of the other rows is done using the same reasoning utilized to derive Long and Yaw. The full matrix that takes the actuation of the BOSEMs and converts that to the Degree of freedom basis is shown below.

Actuation_BOSEMtoDOF =

$$\begin{pmatrix} 0 & 0 & 0 & 1 & 1 & 0 \\ 0 & 0.016 & -0.016 & -0.011 & 0.011 & 0 \\ 0 & 0 & 0 & 0 & 0 & 1 \\ 0.09 & -0.09 & -0.09 & 0 & 0 & 0 \\ 1 & 1 & 1 & 0 & 0 & 0 \\ 0 & 0 & 0 & 0.09 & -0.09 & 0 \end{pmatrix}$$

The above matrix is then inverted to find the actuation matrix, which takes degree of freedom actuation to BOSEM actuation.

3.3.2 Results

The Sensing_DOFtoBOSEM and Actuation_BOSEMtoDOF matrices are then inverted to find the final sensing and actuation matrices.

The sensing matrix takes BOSEM sensing to degree of freedom sensing. It has columns (A,B,C,D,E,F) and rows (Long, Pitch, Side, Roll, Vert, Yaw).

inv(Sensing_DOFtoBOSEM) =
Sensing =

$$\begin{pmatrix} 0 & 0 & 0 & 0.5 & 0.5 & 0 \\ 0 & 31.25 & -31.25 & 0 & 0 & 0 \\ 0 & 0 & 0 & 0 & 0 & 1 \\ 5.5556 & -2.778 & -2.778 & 0 & 0 & 0 \\ 0.5 & 0.25 & 0.25 & 0 & 0 & 0 \\ 0 & 3.8194 & -3.8194 & 5.5556 & -5.5556 & 0 \end{pmatrix}$$

The actuation matrix takes degree of freedom actuation to BOSEM actuation. It has columns (Long, Pitch, Side, Roll, Vert, Yaw) and rows (A, B, C, D, E, F).

inv(Actuation_BOSEMtoDOF) =
Actuation =

$$\begin{pmatrix} 0 & 0 & 0 & 5.5556 & 0.5 & 0 \\ 0 & 31.25 & 0 & -2.778 & 0.25 & 3.8194 \\ 0 & -31.25 & 0 & -2.778 & 0.25 & -3.8194 \\ 0.5 & 0 & 0 & 0 & 0 & 5.5556 \\ 0.5 & 0 & 0 & 0 & 0 & -5.5556 \\ 0 & 0 & 1 & 0 & 0 & 0 \end{pmatrix}$$

The above sensing and actuation matrices are currently used as part of the control and damping system for the Reference Cavity suspension.

3.4 Reference Cavity Suspension Simulation

3.4.1 Transfer Function Simulation

The next step in commissioning the reference cavity suspension is to model the state space and to produce transfer functions. This is done using a matlab Simulink script, written by Bob Taylor. The matlab model enables the behavior of the Reference cavity suspension to be simulated. The transfer functions produced give a mathematical representation, in terms of time frequencies, of the relation between the input and output of the system. In the case of the Reference Cavity suspension the input is the BOSEM actuation and the output is the BOSEM sensing. A triple pendulum system with small motion can also be treated as a linear time-invariant system, which is necessary in order to be able to create a transfer function for the system.

It should be noted that the frequency range was chosen to fit the measurement, and that not all features are shown. Also the lever arms were removed from the Simulink model as the suspensions angular degrees of freedom are already calibrated in radians and newton meters.

3.4.2 Experimental Procedure

For the sake of brevity only the transfer function from roll and sideways motion will be explain in this section. However the same process applies for all coupled and non-coupled degrees of freedom and the results of all the simulations can be found in the results section.

An input signal is injected into the upper mass roll-force/torque input (coil actuator) r-LC-1. The signal is frequency dependently attenuated by the roll loop. Its strength is measured by the readout, displayed in Figure 13. The position of the upper mass in sideways (y1) is measured with another output.

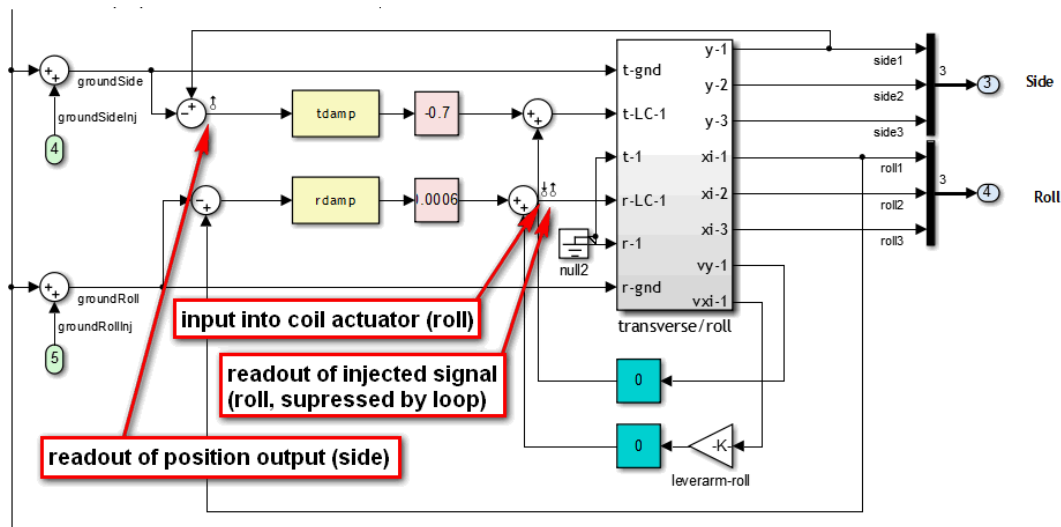


Figure 13 depicts the readout display of the Simulink model used for the Reference Cavity Suspension. It shows where the input signal is injected into the upper mass roll-force/torque input (coil actuator) r-LC-1. It also shows where the signal strength is measured. The position of the upper mass in sideways (y1) is measured with another output depicted above, [Westphal'13].

The system is exactly linearized and the results taken from the Simulink workspace to the matlab workspace for further processing. The results are then accessed in the matlab main window as two state space systems, labeled as linsys with linsys(1) being the first state space and linsys(2) being the second. There is only a single input and a single output per state space system.

Once the state space system has been created the transfer function is then generated. The desired outcome is to know the transfer function from output 1 to output 2. By dividing the transfer functions output1/input1 and output2/input1 one gets output2/output1. This is then plotted. The order one divides (2/1 or 1/2) seems to be quite arbitrary and should be tuned to get a transfer function decreasing towards higher frequencies

3.4.3 Results

Below are the transfer functions produced by the Simulink model as well as a list of the peak frequencies for each plot. The degrees of freedom Long and Pitch, as well as Side and Roll, are strongly coupled due to the geometry of the system. Thus transfer functions between those degrees of freedom are also taken. More discussion will be had on the results from this simulation later on in this paper. They will be compared with the transfer functions measured from the actually suspension.

From the simulation the resonant frequencies are as follows;

Longitudinal

$$f_1 = 2.59 \text{ Hz} \quad f_2 = 1.39 \text{ Hz} \quad f_3 = 0.64 \text{ Hz}$$

Pitch

$$f_1 = 5.198 \text{ Hz} \quad f_2 = 1.88 \text{ Hz} \quad f_3 = 0.9804 \text{ Hz}$$

Side

$$f_1 = 2.622 \text{ Hz} \quad f_2 = 1.392 \text{ Hz} \quad f_3 = 0.640 \text{ Hz}$$

Roll

$$f_1 = 9.11 \text{ Hz} \quad f_2 = 2.264 \text{ Hz}$$

Vertical:

$$f_1 = 4.069 \text{ Hz} \quad f_2 = 1.239 \text{ Hz}$$

Yaw:

$$f_1 = 5.553 \text{ Hz} \quad f_2 = 2.304 \text{ Hz} \quad f_3 = 0.970 \text{ Hz}$$

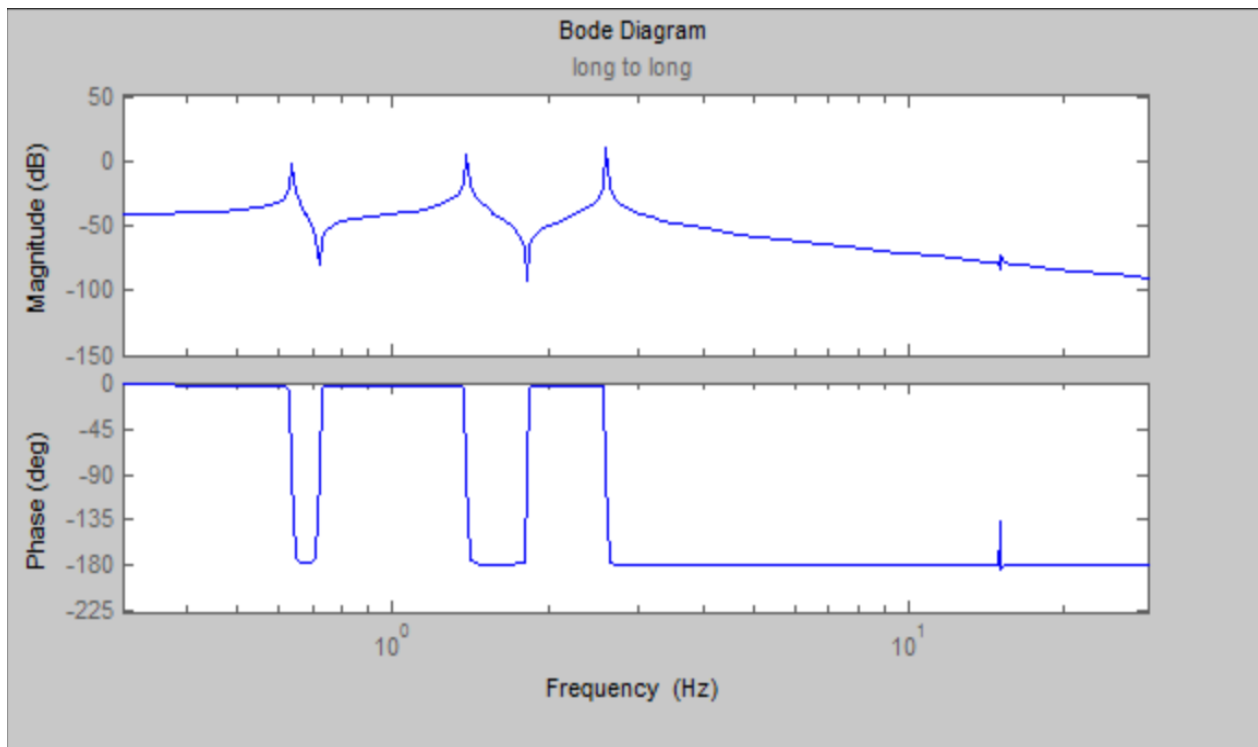


Figure 14 depicts the transfer function simulation from long to long. The resonant frequencies are $f_1 = 2.59$ Hz, $f_2 = 1.39$ Hz and $f_3 = 0.64$ Hz.

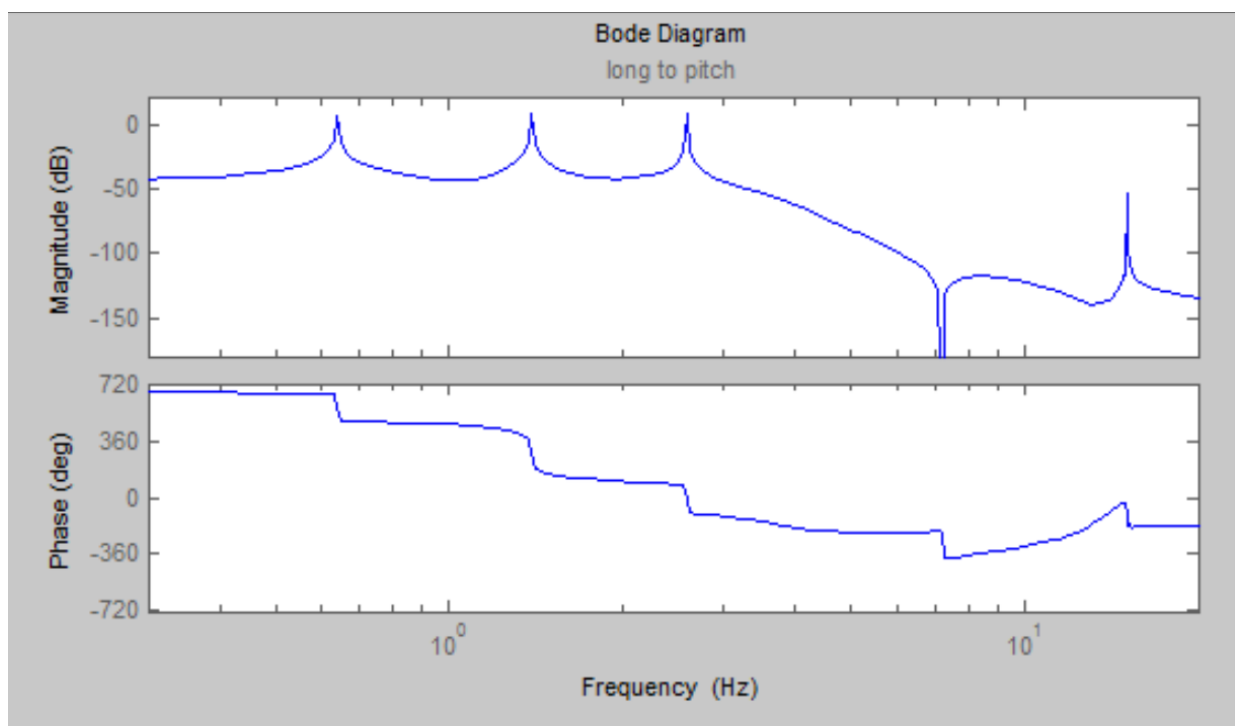


Figure 15 depicts the transfer function simulation from long to pitch. These two degrees of freedom are strongly coupled due to the geometry of the pendulum system.

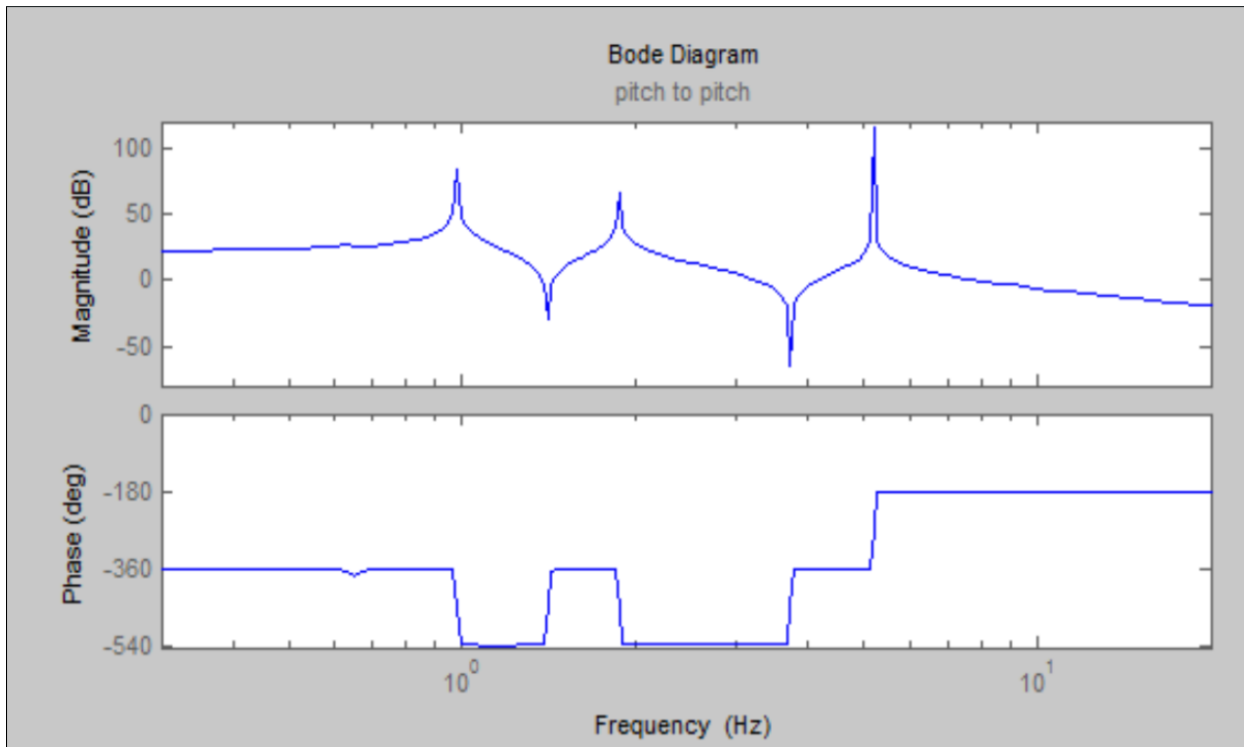


Figure 16 depicts the transfer function simulation from long to long. The resonant frequencies are $f_1 = 5.198$ Hz, $f_2 = 1.88$ Hz and $f_3 = 0.9804$ Hz.

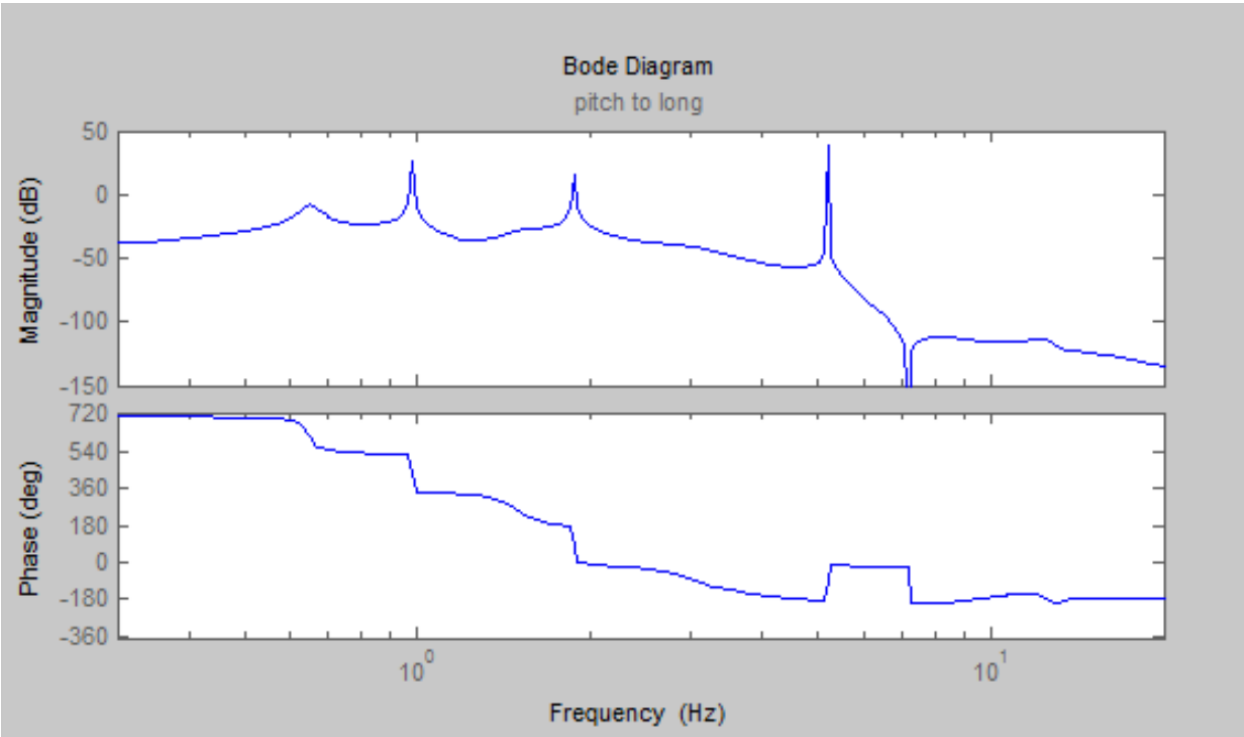


Figure 17 depicts the transfer function simulation system from pitch to long. These two degrees of freedom are strongly coupled due to the geometry of the pendulum system.

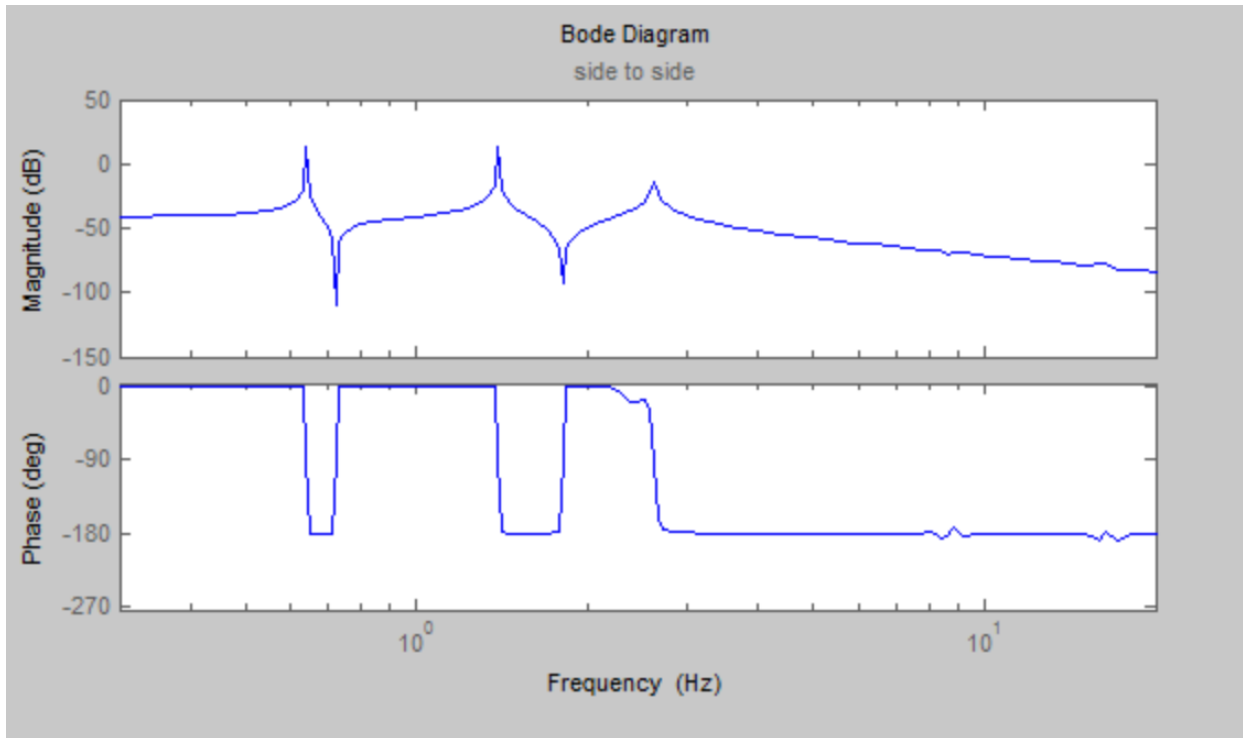


Figure 18 depicts the transfer function simulation from long to long. The resonant frequencies are $f_1 = 2.622$ Hz, $f_2 = 1.392$ Hz and $f_3 = 0.640$ Hz.

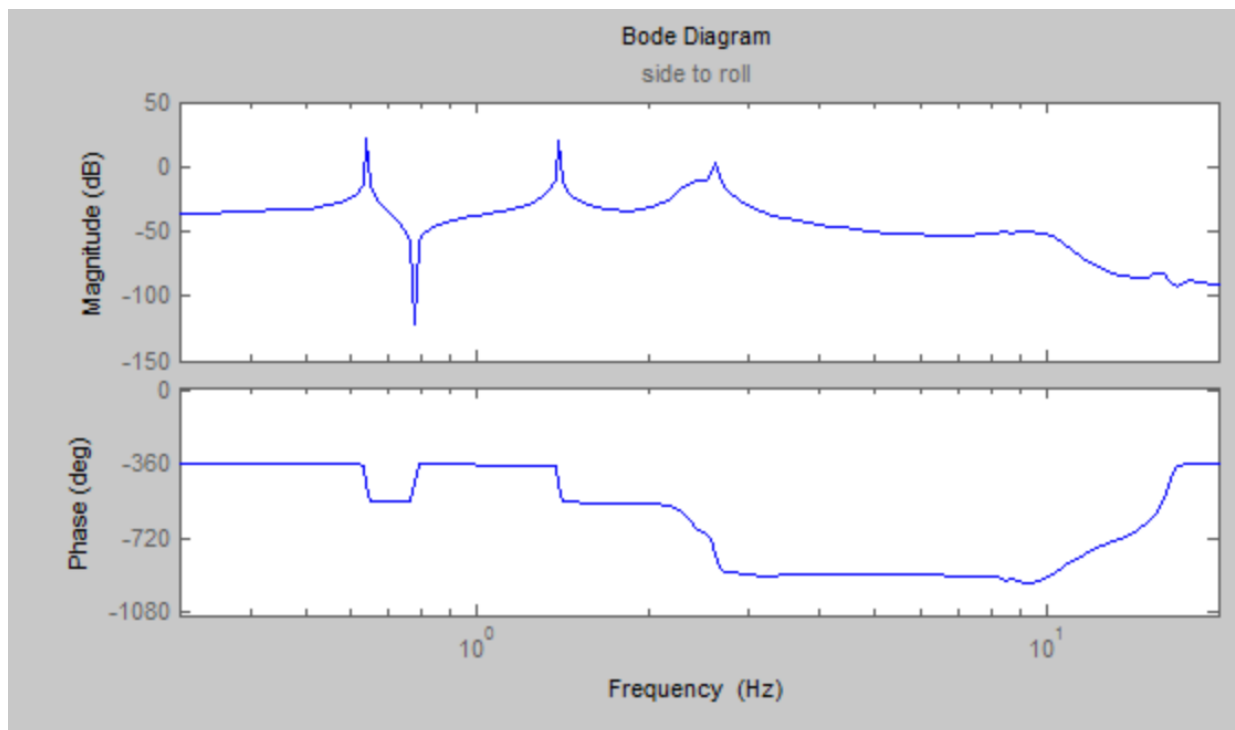


Figure 19 depicts the transfer function simulation from side to roll. These two degrees of freedom are strongly coupled due to the geometry of the pendulum system.

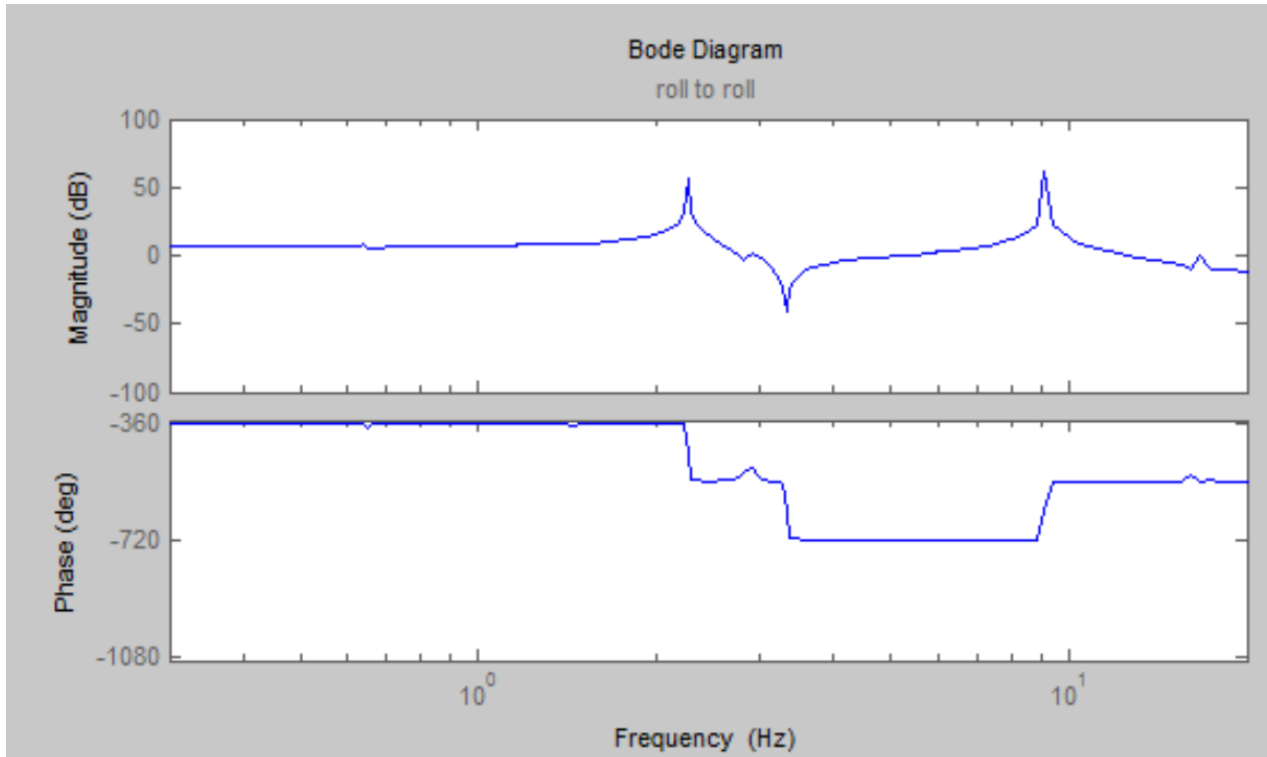


Figure 20 depicts the transfer function simulation from long to long. The resonant frequencies are $f_1 = 9.11$ Hz and $f_2 = 2.264$ Hz.

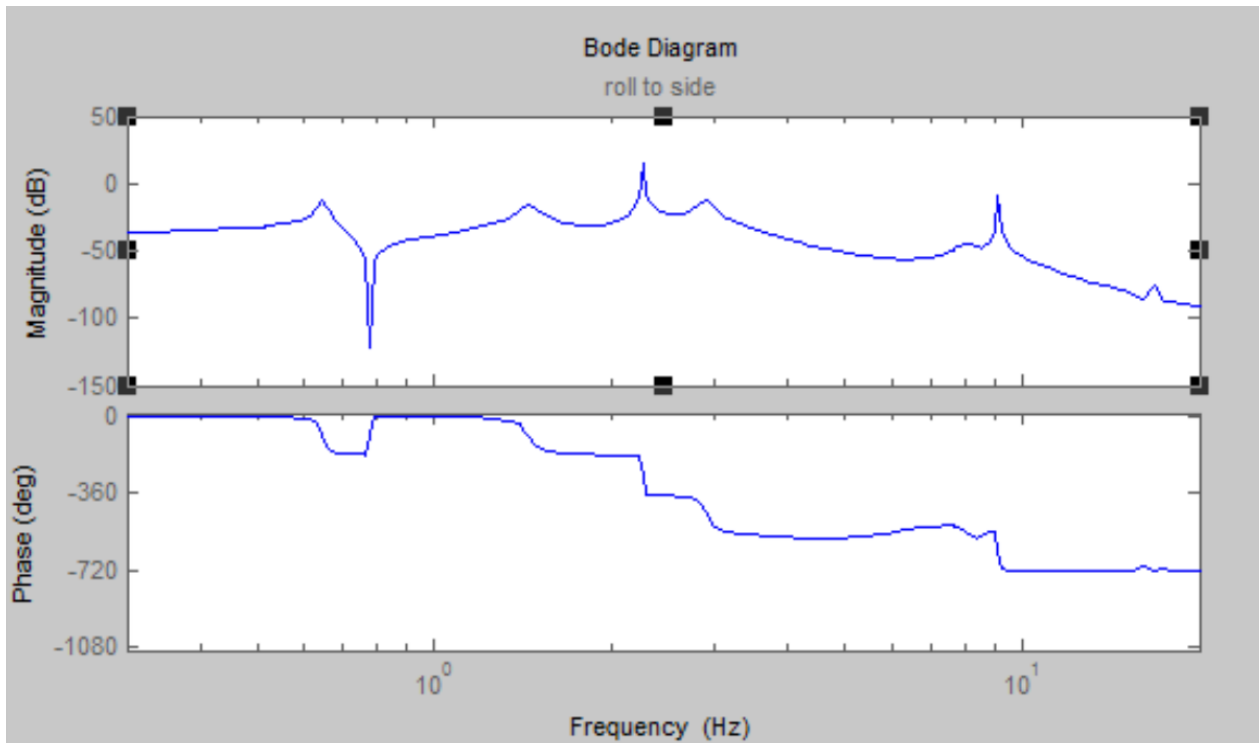


Figure 21 depicts the transfer function simulation from roll to side. These two degrees of freedom are strongly coupled due to the geometry of the pendulum system.

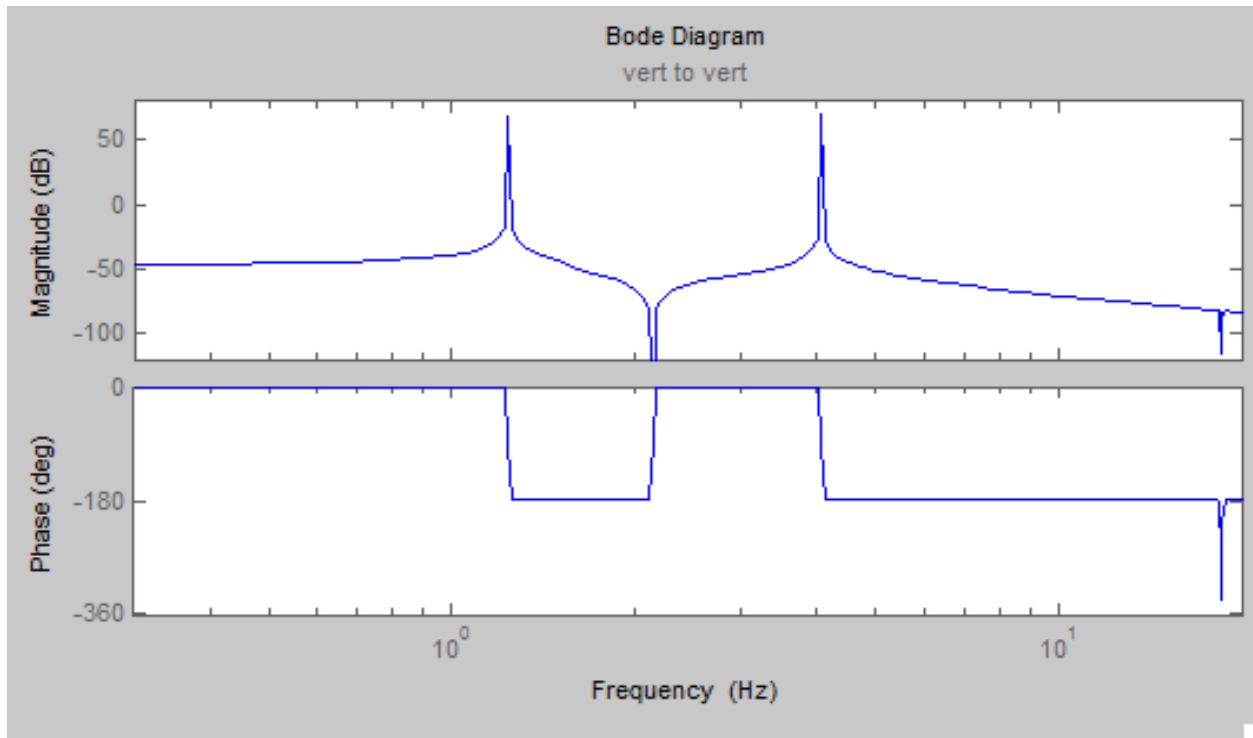


Figure 22 depicts the transfer function simulation from long to long. The resonant frequencies are $f_1 = 4.069$ Hz and $f_2 = 1.239$ Hz.

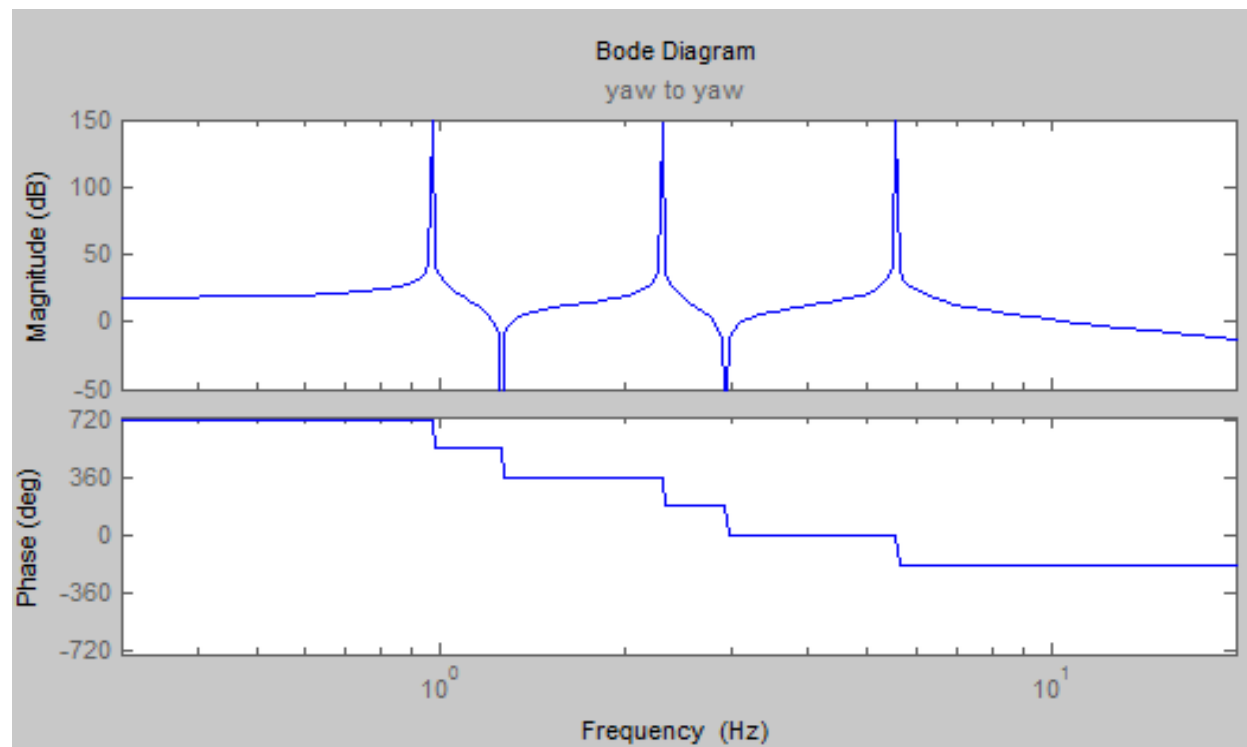


Figure 23 depicts the transfer function simulation from long to long. The resonant frequencies are $f_1 = 5.553$ Hz, $f_2 = 2.304$ Hz and $f_3 = 0.970$ Hz.

3.5 Reference Cavity Suspension Tests

3.5.1 Transfer function

The next step in commissioning the reference cavity suspension is to measure the transfer functions of the suspension. This is done using the Control and Data System (CDS). Using the CDS all 36 transfer functions between the suspension actuators and sensors can be measured. The results section for this test displays six transfer function plots one for each excitations in the degrees of freedom. Just as in the simulated model, the transfer functions produced give a mathematical representation, in terms of time frequencies, of the relation between the input and output of the system.

The CDS digitizes and collects the data from the sensors, controlling the suspension. The CDS used by the 10 m prototype was developed by scientists at the LIGO sites. It provides access to all data collected as well as time-stamping the data with high accuracy for later analysis. The CDS also protects the suspension by avoiding damage from hazardous control signals.

3.5.2 Experimental Procedure

For the sake of brevity only the general manner in which transfer function were measured will be explain in this section. However the same process applies for all coupled and non-coupled degrees of freedom and the results of all the measurement can be found in the results section.

To begin a signal was injected into the upper mass input (coil actuators). The type of input signal used was a series of swept sines in the frequency range of 0.01Hz to 20 Hz. Figure 24 shows the system interface for measurements. To take the measurement, six measurement channels are selected, these measurement channels correspond to the sensing of the six degrees of freedom. For each test one excitation channel is selected, this corresponds to the input of the degree of freedom whose transfer functions are being measured. Once started the test runs overnight. Allowing the test to run overnight assures a more constant temperature as well as fewer disturbances to the suspension.

The strength of the input was chosen in such a way as to insure coherence between the measurement and the output, without over exciting the system. The strength of the input is frequency dependent due to the fact that at higher frequencies, and frequencies near resonance, the motion of the suspension is more sensitive to the input signal.

The excitation was measured by the BOSEM sensors and transformed into the degree of freedom basis as described in section 3.3. For each degree of freedom the transfer function

for sensing over excitation was plotted. In addition, for each excitation the transfer function of the sensing for all other degrees of freedom is also plotted.

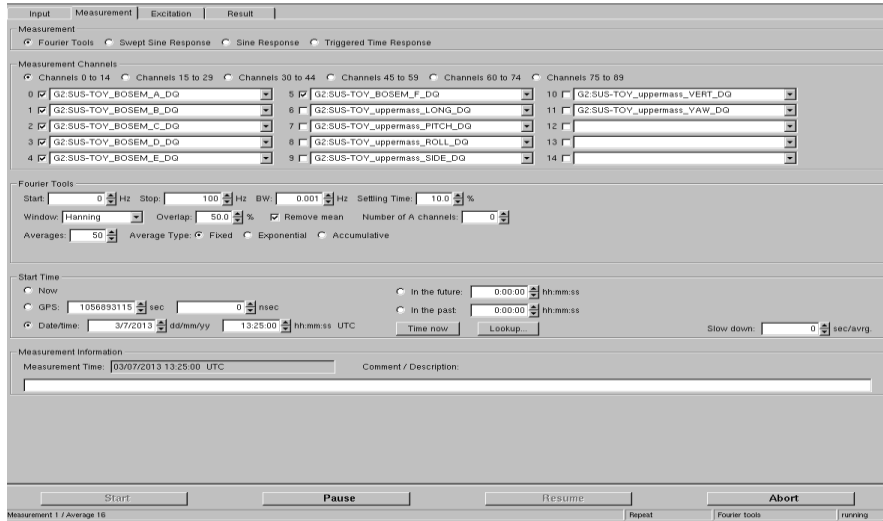


Figure 24 depicts the interface used to measure transfer functions of the reference cavity suspension. Six measurement channels are selected, these measurement channels correspond to the sensing of the six degrees of freedom. For each test one excitation channel is selected this corresponds to the degree of freedom whose transfer functions are being measured. The type of input signal used is a swept sine. The frequencies range is 0.01 Hz to 20 Hz.

3.5.3 Results

Below are the transfer functions measured from the reference cavity suspension as well as a list of the peak frequencies for each plot. The results from this test are compared to the simulated transfer functions in the discussion portion of this section.

From the measurement the resonant frequencies are as follows;

Longitudinal

$$f_1 = 7.893 \text{ Hz} \pm 0.004 \text{ Hz} \quad f_2 = 5.561 \text{ Hz} \pm 0.004 \text{ Hz} \quad f_3 = 2.503 \text{ Hz} \pm 0.004 \text{ Hz} ,$$

$$f_4 = 1.355 \text{ Hz} \pm 0.004 \text{ Hz} \quad f_5 = 0.643 \text{ Hz} \pm 0.004 \text{ Hz}$$

Pitch

$$f_1 = 2.942 \text{ Hz} \pm 0.006 \text{ Hz} \quad f_2 = 4.618 \text{ Hz} \pm 0.004 \text{ Hz} \quad f_3 = 7.89 \text{ Hz} \pm 0.002 \text{ Hz}$$

$$f_4 = 14.668 \text{ Hz} \pm 0.004 \text{ Hz} \quad f_5 = 17.8676 \text{ Hz} \pm 0.004 \text{ Hz}$$

Side

$$f_1 = 0.679 \text{ Hz} \pm 0.004 \text{ Hz} \quad f_2 = 1.03687 \text{ Hz} \pm 0.05 \text{ Hz} \quad f_3 = 3.0261 \text{ Hz} \pm 0.007 \text{ Hz}$$

$$f_4 = 3.686 \text{ Hz} \pm 0.004 \text{ Hz}$$

Roll

$$f_1 = 1.12 \text{ Hz} \pm 0.05 \text{ Hz} \quad f_2 = 3.026 \text{ Hz} \pm 0.006 \text{ Hz} \quad f_3 = 3.7915 \text{ Hz} \pm 0.004 \text{ Hz}$$

$$f_4 = 4.61847 \text{ Hz} \pm 0.007 \text{ Hz} \quad f_5 = 7.89 \text{ Hz} \pm 0.004 \text{ Hz}$$

Vertical:

$$f_1 = 0.679 \text{ Hz} \pm 0.004 \text{ Hz} \quad f_2 = 1.03687 \text{ Hz} \pm 0.02 \text{ Hz} \quad f_3 = 3.1126 \text{ Hz} \pm 0.006 \text{ Hz}$$

$$f_4 = 3.58368 \text{ Hz} \pm 0.004 \text{ Hz}$$

Yaw:

$$f_1 = 0.9263 \text{ Hz} \pm 0.004 \text{ Hz} \quad f_2 = 1.49575 \text{ Hz} \pm 0.004 \text{ Hz} \quad f_3 = 3.0261 \text{ Hz} \pm 0.006 \text{ Hz}$$

$$f_4 = 4.49011 \text{ Hz} \pm 0.004 \text{ Hz} \quad f_5 = 7.89 \text{ Hz} \pm 0.004 \text{ Hz}$$

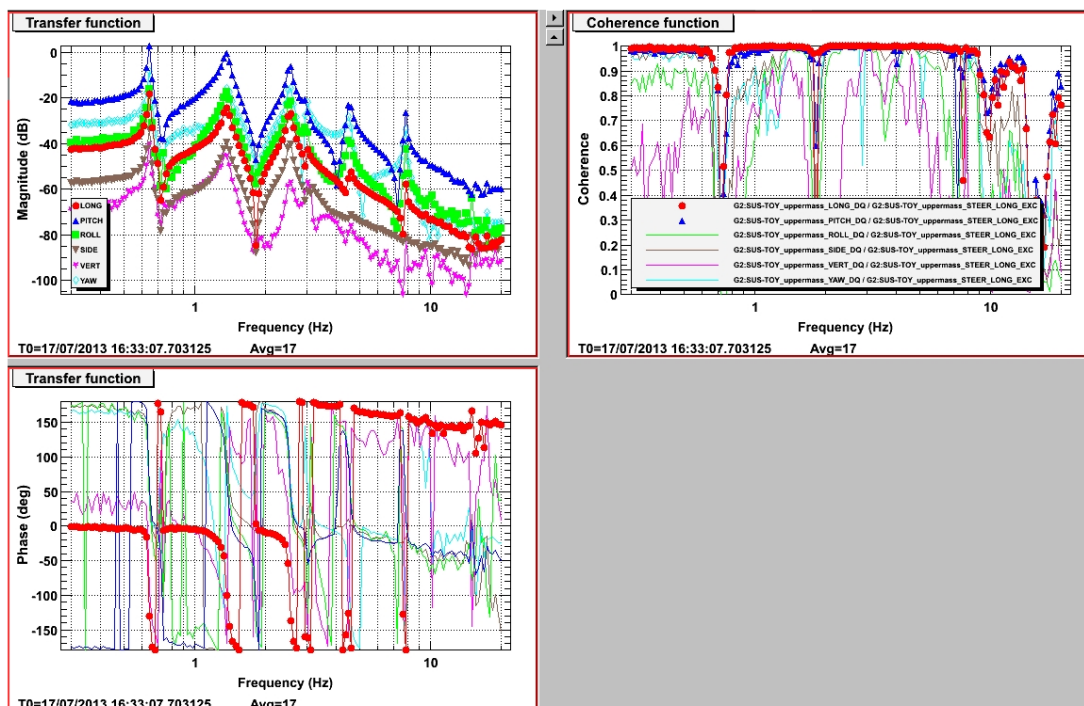


Figure 25 depicts the transfer function simulation from long to long. The resonant frequencies are $f_1 = 5.561 \text{ Hz} \pm 0.004 \text{ Hz}$, $f_2 = 5.561 \text{ Hz} \pm 0.004 \text{ Hz}$, $f_3 = 2.503 \text{ Hz} \pm 0.004 \text{ Hz}$, $f_4 = 1.355 \text{ Hz} \pm 0.004 \text{ Hz}$, and $f_5 = 0.643 \text{ Hz} \pm 0.004 \text{ Hz}$.

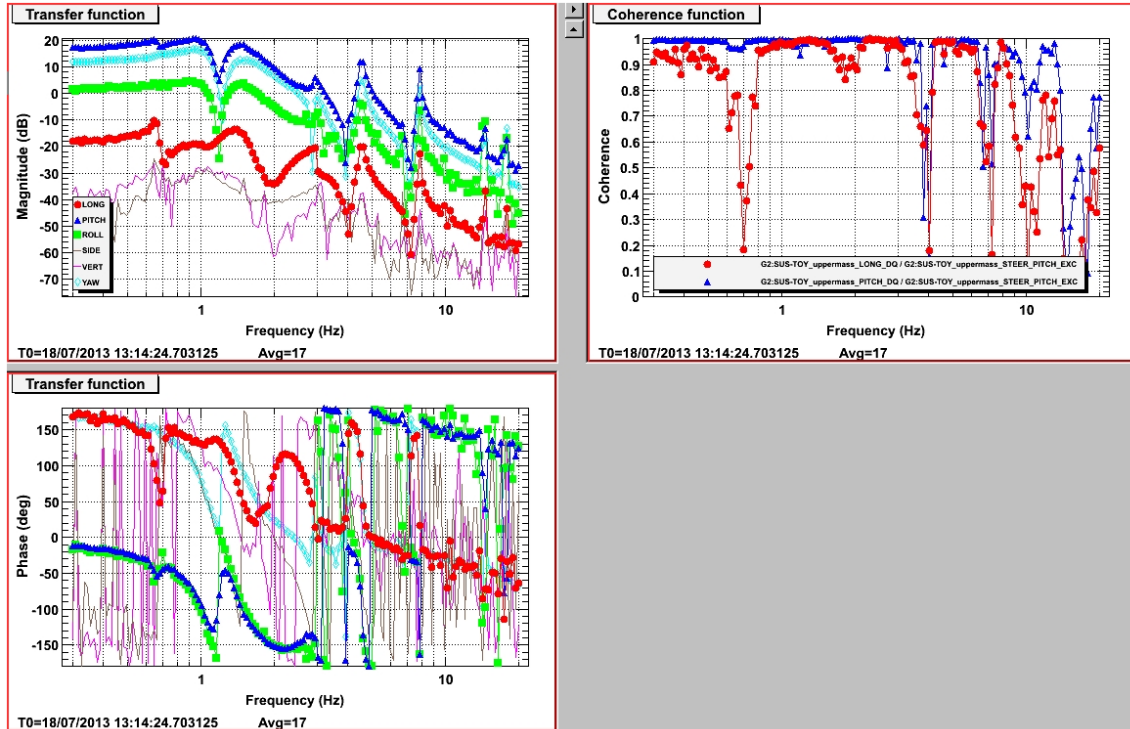


Figure 26 depicts the transfer function simulation from Pitch to Pitch. The resonant frequencies are $f_1 = 2.942 \text{ Hz} \pm 0.004 \text{ Hz}$, $f_2 = 4.618 \text{ Hz} \pm 0.004 \text{ Hz}$, $f_3 = 7.89 \text{ Hz} \pm 0.004 \text{ Hz}$, $f_4 = 14.668 \text{ Hz} \pm 0.004 \text{ Hz}$, $f_5 = 17.8676 \text{ Hz} \pm 0.004 \text{ Hz}$.

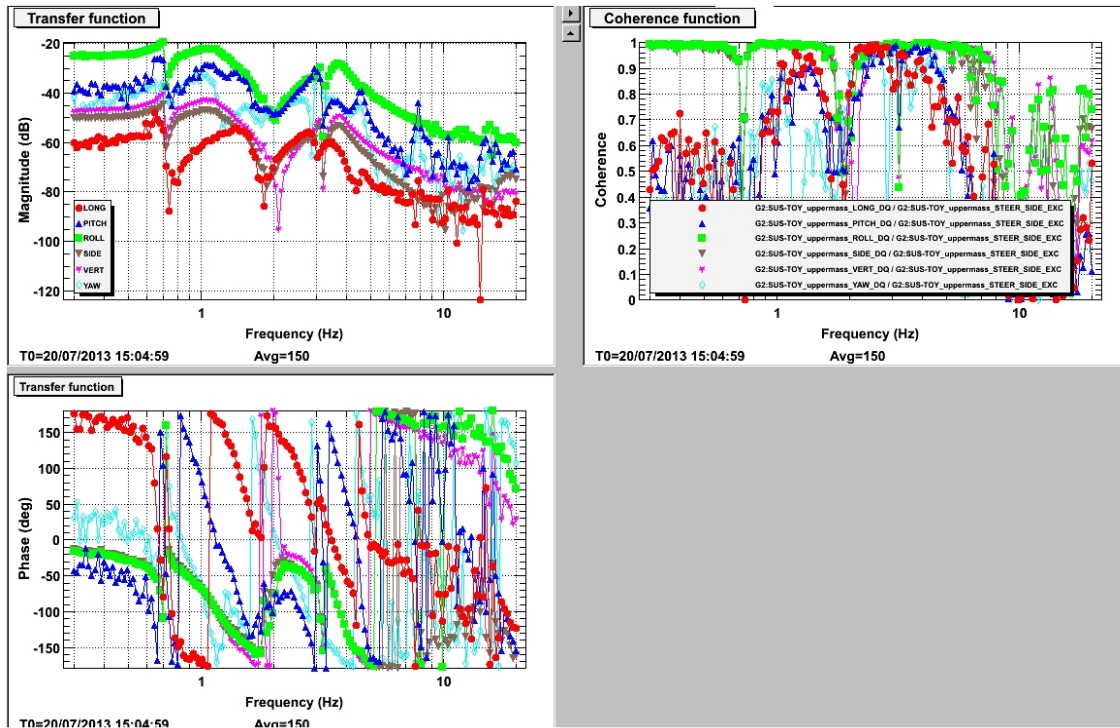


Figure 27 depicts the transfer function simulation from side to side. The resonant frequencies are $f_1 = 0.679 \text{ Hz} \pm 0.004 \text{ Hz}$, $f_2 = 1.03687 \text{ Hz} \pm 0.004 \text{ Hz}$, $f_3 = 3.0261 \text{ Hz} \pm 0.004 \text{ Hz}$ and $f_4 = 3.686 \text{ Hz} \pm 0.004 \text{ Hz}$.

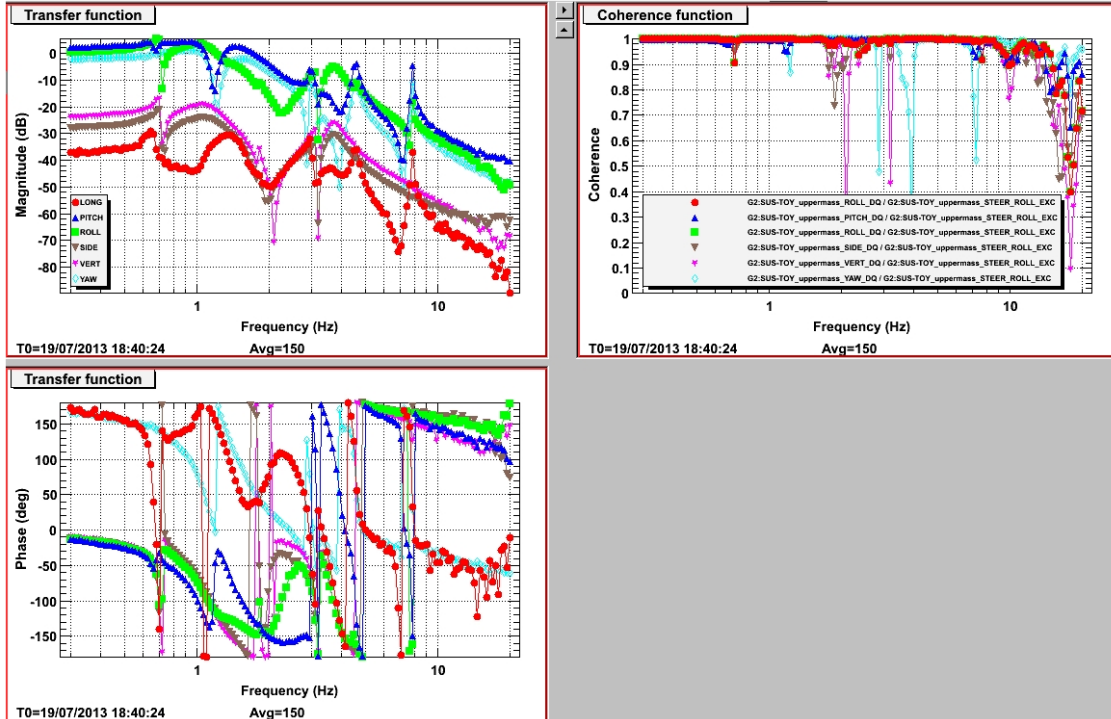


Figure 28 depicts the transfer function simulation from roll to roll. The resonant frequencies are $f_1 = 1 \text{ Hz} \pm 0.004 \text{ Hz}$, $f_2 = 3.026 \text{ Hz} \pm 0.004 \text{ Hz}$, $f_3 = 3.7915 \text{ Hz} \pm 0.004 \text{ Hz}$, $f_4 = 4.61847 \text{ Hz} \pm 0.004 \text{ Hz}$ and $f_5 = 7.89 \text{ Hz} \pm 0.004 \text{ Hz}$.

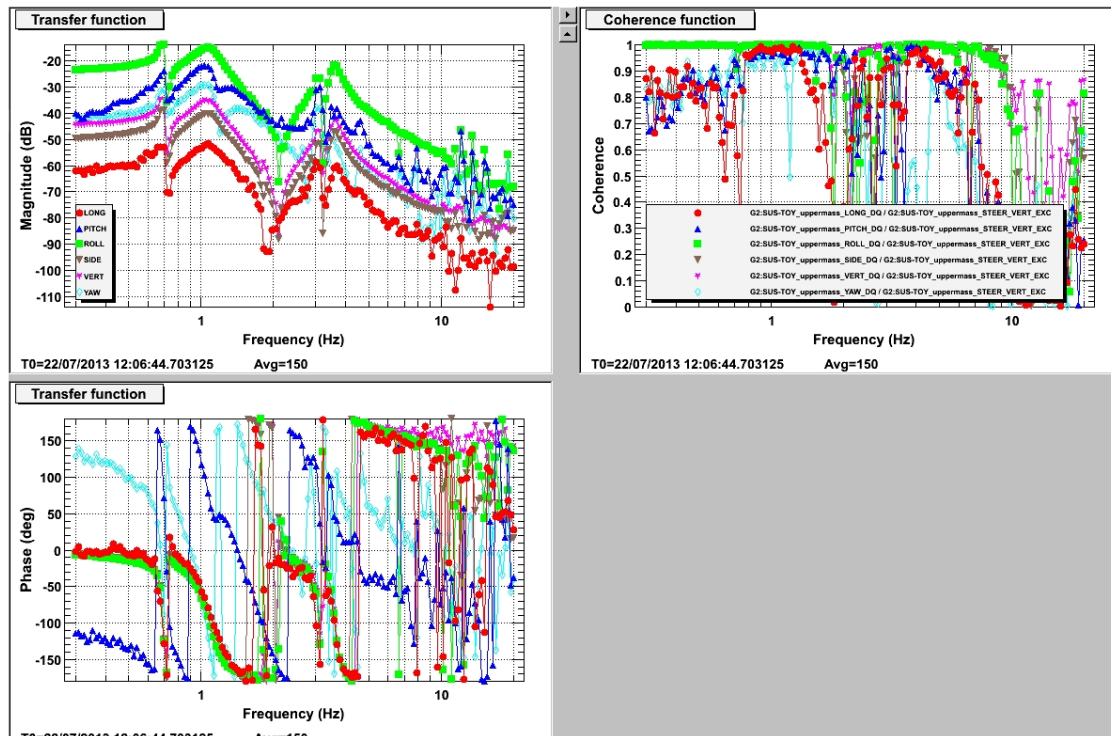


Figure 29 depicts the transfer function simulation from vert to vert. The resonant frequencies are $f_1 = 0.679 \text{ Hz} \pm 0.004 \text{ Hz}$, $f_2 = 1.03687 \text{ Hz} \pm 0.004 \text{ Hz}$, $f_3 = 3.1126 \text{ Hz} \pm 0.004 \text{ Hz}$, $f_4 = 3.58368 \text{ Hz} \pm 0.004 \text{ Hz}$.

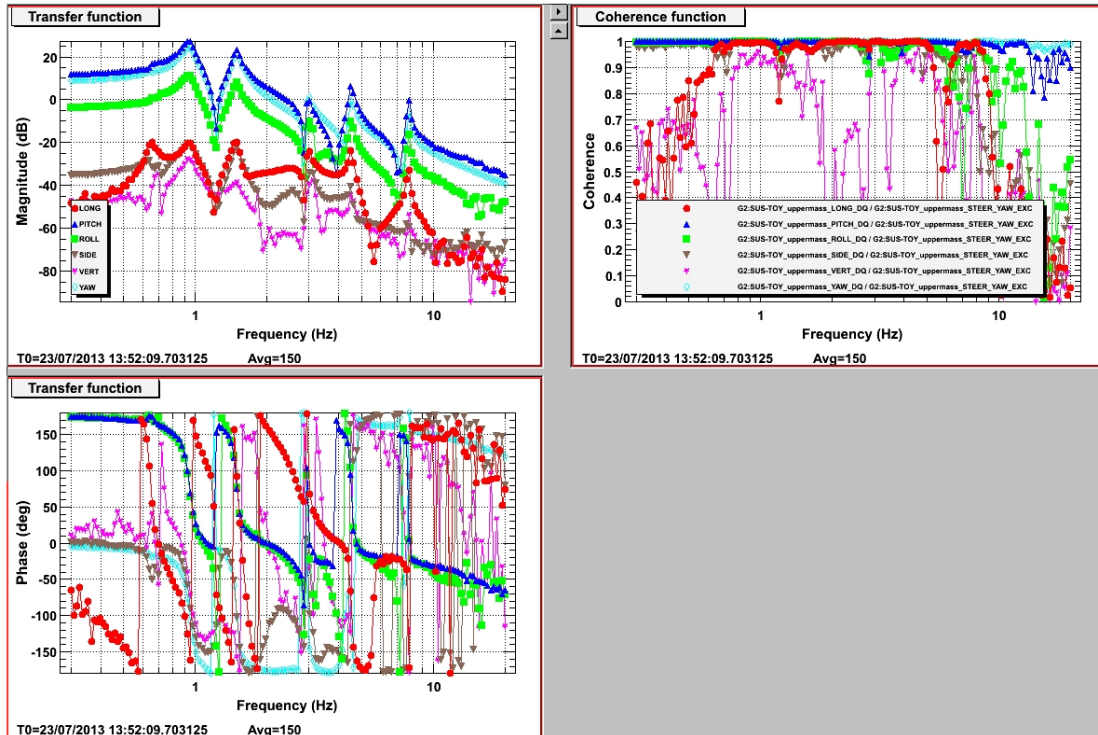


Figure 30 depicts the transfer function simulation from yaw to yaw. The resonant frequencies are $f_1 = 0.9263 \text{ Hz} \pm 0.004 \text{ Hz}$, $f_2 = 1.49575 \text{ Hz} \pm 0.004 \text{ Hz}$, $f_3 = 3.0261 \text{ Hz} \pm 0.004 \text{ Hz}$, $f_4 = 4.49011 \text{ Hz} \pm 0.004 \text{ Hz}$ and $f_5 = 7.89 \text{ Hz} \pm 0.004 \text{ Hz}$.

3.5.4 Discussion

Looking at figures 25-30 it's clear that the measured transfer functions are not of high quality. For example compare figure 14, the simulation of the longitudinal transfer function, and figure 25 the measured transfer function of longitudinal. The simulation depicts three distinct resonances while the measured transfer function has five. The poor quality is even more pronounced in figure 26, the measured transfer function of pitch. The figure displays several broad peaks as opposed to the sharp resonances found in the simulation. These sorts of features are apparent in all of the measured transfer functions. It is also more often the case that the resonance for the simulated transfer functions and the measured are not the same. In general the simulated transfer functions do not match the measured.

There are a great number of possible factors that could be contributing to this disagreement between the measured and simulated transfer functions. They included the following;

- Incorrect Matlab Model
- Damping of Resonants
- Magnetic Cross talk between BOSEMs
- Issues with the BOSEM sensing
- Issues with the BOSEM actuation

Extra mass was added to the upper mass of the reference cavity suspension in order to make it more stable during the commissioning. This along with other parameters are not accounted for in the simulated model. This disparity between the parameters used by the Matlab model and the actual suspension may account for the non-agreement of the resonant frequencies.

Damping of the upper mass is on during the measurement. This may account for some of the broader resonants. As the upper mass rings up the local damping kicks in and you measure a less defined peak in the transfer function.

It was shown in section 3.2.3 that there is Magnetic Cross talk between BOSEMs on the upper mass. This magnetic crosstalk is causing coupling between different degrees of freedom. This coupling may be the source of the additional resonances as an excitation in one degree of freedom may excite another due to the magnetic cross couplings. This phenomenon may explain the additional resonances in the measured transfer functions. Unfortunately this coupling of the BOSEMs is not well understood and it is not clear from the figures which degrees of freedom are effecting the transfer functions of the others.

It was also found in section 3.2 that there were some issue with the sensor gain of the BOSEMs, this would affect what values are measured and produce further coupling of the degrees of freedom. The BOSEM sensing is used to deduce the BOSEM actuation, issues with the sensing cast a shadow on the reliability of the actuation.

All these factors plus possible unknown sources cause the quality of the measured transfer functions to be poor. Though the results are less than desirable there are steps that can be taken to improve the measurement and ultimately produce transfer functions that are accurately modeled and known.

The commissioning of the reference cavity suspension is ongoing. Further tests measuring the motion of the mass without using the BOSEM sensing to characterize the BOSEM actuation are currently be conducted. Once the BOSEM actuation is known future test will use this to characterize the BOSEM sensing. The Matlab script will be refined and parameters corrected. Finally a correction matrix will be created to account for the magnetic crosstalk in BOSEMs. Once these steps have been implemented the transfer functions will be both simulated and measured again for further comparison.

4 Conclusion

4.1 The 10 m Prototype Commissioning, Moving Forward

This report presents the work done modeling and testing the reference cavity suspension for the 10 m prototype detector at the Albert Einstein Institute, Hannover, Germany.

The 10 m prototype is designed to perform experiments at or below the Standard Quantum Limit. In order for the interferometer to operate at such levels of sensitivity it must be isolated from seismic and thermal noise. In order to reach the desired sensitivities the 10 m prototype utilizes seismically isolated benches that will be interferometrically interconnected and stabilized. The interferometer will be placed within a ultra-high vacuum system. It also utilizes multi pendulum suspensions with cantilever springs. The sensitivity of the 10 m prototype enables it to be used for experiments in the field of macroscopic quantum mechanics.

The reference cavity suspension of the 10 m prototype is one of several subsystems. The triple pendulum system utilized by the reference cavity suspension incorporates two stages of cantilever springs, the design effectively isolates the test masses from seismic motion. A detailed dynamical model for a triple pendulum suspension was described in this report. The model can be used to investigate the mode frequencies, transfer functions or impulse response for all degrees of freedom, among other things. This is essential for the design of a well damped triple pendulum with minimal coupling between modes.

Experiments on the reference cavity suspension are described in this report. The BOSEM actuation and sensing was tested and magnetic cross talk between the BOSEMs was found. The transfer functions of the suspension were modeled using matlab and the results were compared to the measurements of the transfer functions of the suspension. It was found that the measured and modeled transfer functions did not agree. The primary reasons for this disagreement are magnetic cross talk between BOSEMs, incorrect parameters in the Matlab model, and poor characterization of the BOSEM sensing and actuation.

Currently the commissioning of the 10 m prototype is ongoing. Further tests characterizing the reference cavity suspension are being conducted. In addition to the reference cavity progress in other subsystems is being made and the commissioning of the prototype is making progress. The Vacuum system is installed and working. Two of the three tables, part of the AEI SAS seismic Isolation, are installed and working. The advanced LIGO 35 W laser is currently coupled into the vacuum and is installed and functioning. The suspension Platform interferometer has been installed for one degree of freedom. In the near future a single arm test will be conducted for the 10 m prototype, with the goal of learning to cope with the marginal stability the instrument operates with. Work towards the goal of a fully realized 10 m prototype operating at the SQL is making headway. The 10 m prototype is on track to conduct experiments at or below the standard quantum limit.

4.2 Acknowledgments

I would like to thank Prof. Bernard Whiting, Prof Guido Mueller, and the University of Florida Physics Department for accepting me in the IREU program. Antonis Mytidis and Krisitn Nichola for arranging all my travel and finances, and checking in on me during my travels. Prof. Laura Cadonati for mentoring me, and assisting me in becoming a part of this program. Prof. Stefan Goßler, Dr. Tobin Fricke, Tobias Westphal and all of my colleagues at the Albert Einstein Institute in Hannover for allowing me to work with them and so seamlessly incorporating me into their group. Finally I would like to thank the National Science Foundation for funding the IREU program. Without their support, none of this would have been possible.

References

- [Bradashia'90] C. Brandashia et al. 1990 *Nuclear Instruments and Methods in Physics Research A* 289 518-525.
- [Cumming'12] Cumming, Alan, Liam Cunningham, Stefan Goßler, Giles Hammond, Russell Jones, Ken Strain, Marielle Van Veggel, and Tobias Westphal. *Suspension System for the AEI 10 M Prototype*. Hannover, Germany: Max-Planck-Institut Fur Gravitationsphysik (AEI), 2012. Print.
- [Dahl'12] Dahl, K., T. Alig, G. Bergmann, A. Bertolini, M. Born, Y. Chen, A. V. Cumming, L. Cunningham, C. Gräf, G. Hammond, G. Heinzel, S. Hild, S. H. Huttner, R. Jones, F. Kawazoe, S. Köhlenbeck, G. Kühn, H. Lück, K. Mossavi, P. Oppermann, J. Pöld, K. Somiya, A. A. Van Veggel, A. Wanner, T. Westphal, B. Willke, K. A. Strain, S. Goßler, and K. Danzmann. *Status of the AEI 10 M Prototype*. Tech. Hannover, Germany: Max-Planck-Institut Fur Gravitationsphysik (AEI), 2012. Print.
- [Danzmann'95] K. Danzmann et al 1995 in *First Edoardo Amaldi Conference on Gravitational Wave Experiments Frascati 1994*, (World Scientific, Singapore) 100-111
- [Einstien'16] Einstein, Albert. *Relativity: The Special and General Theory*. Tech. Trans. Robert W. Lawson. N.p.: Methuen & Co, 1916. Print.
- [Forward'78] R.L. Forward, *Phys. Rev. D*, 17, (1978), 379.
- [Goßler'10] Goßler, S., A. Bertolini, M. Born, Y. Chen, K. Dahl, C. Gräf, G. Heinzel, S. Hild, F. Kawazoe, O. Kranz, G. Kühn, H. Lück, K. Massavi, R. Schanbel, K. Somiya, K. A. Strain, J. R. Taylor, A. Wanner, T. Westphal, B. Willke, and K. Danzmann. *The AEI 10 M Prototype Interferometer*. Tech. 8th ed. Vol. 27. N.p.: IOP Science Logo, 2010. Print. Classical and Quantum GravityEmail Alert RSS Feed.
- [Goßler'68] Goßler, Stefan. *The Suspension System of the Interferometric Gravitational-wave Detector GEO 600*. Thesis. University of Hannover, 1968. Hannover, Germany: Vom Fachbereich Physik Der Universität Hannover, 1968. Print.
- [Ju'04] L.Lu,P.Barriga,D. G. Blair, A. Brooks, R. Burston, X. T. Chin, E. J. Chin, C. Y. Lee, D, Coward, B. Cusack, G. de Vine, J. Degallaix, J.C. Dumas, F. Garoi, S. Gras, M. Gray, D. Hosken, E. Howell, D. Mudge, J. Munch, S. Schediwy, S. Scott, A. Searle, B. sheard, B. Slagmolen, P. Veitch, J. Winterfloor, A. Wooley, Z. Yan, C. Zhai 2004 *ACIGA's high optical test power test facility* *Class. Quantum Grav.* 21 887-893
- [Sigg'04] D. Sigg 2004 *Commissioning of the LIGO detectors* *Class. Quantum Grav.* 21 409-416

- [Somiya,Kentaro'12] Somiya, and Kentaro. *Detector Configuration of KAGRA-the Japanese Cryogenic Gravitational-wave Detector*. Tech. 12th ed. Vol. 29. N.p.: Classical and Quantum Gravity, 2012. Print. Classical and Quantum Gravity.
- [Stochino'09] Stochino A et al 2009 Nucl. Instrum. Methods A 598 737
- [Takahashi'04] R. Takahashi and the TAMA Collaboration 2004 *The Status of TAMA300 Class*. Quantum Grav. **21** 403-408
- [Torrie'01] Torrie, Calum I. E. *Development of Suspension For The GEO 600 Gravitational Wave Detector*. Thesis. University of Glasgow, 2001. Glasgow: University of Glasgow, 2001. Print.
- [Vitale'02] S. Vitale, P. Bender, A. Brillet, S. Buchman, A. Cavalleri, M. Cerdonio, M. Cruise, C. Cutler, K. Danzmann, R. Dolesi, W. Folkner, A. Gianolio, Y. Jafry, G. Hasinger, G. Heinzel, C.Hogan, M. Hueller, J. Hough, S. Phinney, T. Prince, D. Richstone, D. Robertson, M. Rodrigues, A. Rüdiger, M. Sandford, R. Schilling, D. Shoemaker, B. Schutz, R. Stebbins, C. Stubbs, T. Sumner, K. Thorne, M. Tinto, P. Touboul, H.Ward, W. Weber, W. Winkler 202 *LISA and its in-flight test precursor SMART-2* Nucl. Phys. B-Proc. Suppl. **110** 209-216
- [Weiss'72] R. Weiss, M.I.T. Quarterly Progress Report No. 105, (1972).
- [Westphal'11] Westphal, Tobias. "The AEI 10m Prototype Interferometer." LVC Meeting. Gainesville. Sept. 2011. Lecture.
- [Westphal'13] Westphal, Tobias. Upper Mass of Reference Cavity Suspension Degrees of Freedom. Digital image. *RefC Upper Mass & Coils Coordinate System*. Albert Einstein Institute, 25 Feb. 2013. Web.

Appendix A. Simulink Model Parameters

A1. Script Title: global_constants.m

Author: Bob Taylor

Date last modified: 05/08/09

This script generates a global variable "constants", where sub-variables represent categories of constant. For example; constants.fundamental, constants.optical, constants.material etc; and sub-sub variables represent appropriate quantities. Examples of sub-sub variables include; constants.fundamental.h = $6.63 \cdot 10^{-34}$.

More specific pendulum parameters are stored in a pend global variable, generated by build_pend.m.

GLOBAL CONSTANTS

FUNDAMENTAL

constants.fundamental.e0 = 8.8541878176e-12;	F/m; Permittivity of Free Space
constants.fundamental.hbar = 1.054572e-34;	J-s; (Plancks constant)/(2*pi)
constants.fundamental.c = 2.99792458e8;	m/s; Speed of light in Vacuum
constants.fundamental.G = 6.67259e-11;	m ³ /Kg/s ² ; Grav. Constant
constants.fundamental.kB = 1.380658e-23;	J/K; Boltzman Constant
constants.fundamental.h = constants.fundamental.hbar*2*pi;	J-s; Plancks constant
constants.fundamental.R = 8.31447215;	J/(K*mol); Gas Constant
constants.fundamental.g = 9.81;	m/s ² ; grav. acceleration

INFRASTRUCTURE

constants.infrastructure.temp = 273.15 + 20;	Room temperature in the lab
constants.infrastructure.fs = 16384;	Sampling frequency (Hz)
constants.infrastructure.length = 11.65;	meters
constants.infrastructure.residualGas.pressure = 4.0e-7;	Pa
constants.infrastructure.residualGas.mass = 3.34765e-27;	kg;
constants.infrastructure.residualGas.polarizability = 7.81917*10 ⁻³¹ ;	m ³ ;

LASER

constants.laser.wavelength = 1.064e-6;	Laser wavelength
constants.laser.inputPower = 30;	Input power

OPTICS

constants.optics.loss = 37.5e-6;

Typical average per mirror
power loss

constants.optics.PDefficiency = 0.9;

Photodetector efficiency

SEISMIC

constants.seismic.kneeFrequency = 5;

Seismic roll-off frequency

constants.seismic.baseLevel = 1e-7;

Value in m/rt(Hz) at DC

constants.seismic.preisol.attenuationH = 70;

Attenuation from pre isolation, in dB, in h
direction

constants.seismic.preisol.peakfreqH = 0.1;

Resonant peak of preisol system in h

constants.seismic.preisol.peakQH = 8;

Q of this peak

constants.seismic.preisol.attenuationV = 60;

Attenuation from preisolation, in dB, in v
direction

constants.seismic.preisol.peakfreqV = 0.2;

Resonant peak of preisol system in v

constants.seismic.preisol.peakQV = 8;

Q of this peak

MATERIALS

Silica (bulk)

constants.materials.silica.rho = 2.2e3;

kg/m³;

constants.materials.silica.C = 772;

J/kg/K;

constants.materials.silica.k = 1.38;

W/m/K, thermal conductivity

constants.materials.silica.alpha = 3.9e-7;

1/K;

constants.materials.silica.dlnYdT = 1.52e-4;

(1/K), dlnY/dT

constants.materials.silica.phi = 4.1e-10;

constants.materials.silica.Y = 7.2e10;

Pa; Youngs Modulus

constants.materials.silica.dissdepth = 1.5e-2;

constants.materials.silica.sigma = 0.167;

Poisson ratio

constants.materials.silica.Cv = 1.6412e6;

Crooks et al, Fejer et al (Cv=
rho*C)

constants.materials.silica.n = 1.45;

Refractive index

constants.materials.silica.c2 = 7.6e-12;

Coeff of freq depend. term

for

bulk mechanical loss,

7.15e-12 for Sup2

constants.materials.silica.mechanicalLossExponent=0.77;

Exponent for freq
dependence of silica loss,
0.822 for Sup2

Silica (coating)

constants.materials.silica.coating.alpha = 5.1e-7;
constants.materials.silica.coating.beta = 8e-6;
constants.materials.silica.coating.k = constants.materials.silica.k;
constants.materials.silica.coating.phi = 4.0e-5;

dn/dT
Thermal conductivity
coating loss

Tantala (coating)

constants.materials.tantala.coating.Y = 140e9;
constants.materials.tantala.coating.sigma = 0.23;
constants.materials.tantala.coating.Cv = 2.1e6;
constants.materials.tantala.coating.alpha = 3.6e-6;
constants.materials.tantala.coating.beta = 1.4e-5;
constants.materials.tantala.coating.k = 33;
constants.materials.tantala.coating.phi = 2.3e-4;
constants.materials.tantala.coating.n = 2.06539;

C70 Steel

constants.materials.C70Steel.Rho = 7800;
constants.materials.C70Steel.C = 486;
constants.materials.C70Steel.k = 49;
constants.materials.C70Steel.Alpha = 12e-6;
constants.materials.C70Steel.dlnYdT = -2.5e-4;
constants.materials.C70Steel.Phi = 2e-4;
constants.materials.C70Steel.Y = 212e9;
constants.materials.C70steel.breakingStress = 2.9e9;

Tungsten / Wolfram

constants.materials.tungsten.Rho = 19300;
constants.materials.tungsten.C = 134;
constants.materials.tungsten.k = 163.3;
constants.materials.tungsten.Alpha = 4.4e-6;
constants.materials.tungsten.dlnYdT = -9.64e-5;
constants.materials.tungsten.Phi = 1/2e5;
constants.materials.tungsten.Phi = 1/1e4;
constants.materials.tungsten.Y = 400e9;
constants.materials.tungsten.breakingStress = 3.7e9;
constants.materials.tungsten.sigma = 0.28;

California Spring Steel

constants.materials.californiaSpringSteel.Y = 2.2e11;

Marval 18 Maraging Steel

constants.materials.maragingSteel.Rho = 8000;
constants.materials.maragingSteel.C = 460;
constants.materials.maragingSteel.k = 20;

Assumes annealed

```
constants.materials.maragingSteel.Alpha = 11e-6;
constants.materials.maragingSteel.dlnYdT = 0;
constants.materials.maragingSteel.Phi = 1e-4;
constants.materials.maragingSteel.Y = 186e9;
constants.materials.maragingSteel.sigma = 0.3;
```

standard assumption for blades
Assumes annealed

```
Stainless steel grade 302
constants.materials.Steel302.Y = 1.65e11;
```

```
Stainless steel grade 316
contains more carbon (~0.8%) than regular 302, is harder etc
constants.materials.Steel316.Y = 1.93e11;
```

```
Aluminium
constants.materials.aluminium.rho = 2700;
```

A2. Script Title: build_pend.m

Author: Bob Taylor
Date last modified: 05/08/09

More specific pendulum parameters are stored in a pend global variable, generated by build_pend.m.

PENDULUM

UPPER MASS

```
pend.m1_parameters = 'inventor calculated';
pend.material1 = 'stainless steel';
pend.m1 = 0.995;
pend.l1x = 3.206664e-4;
pend.l1y = 6.34485e-4;
pend.l1z = 2.976341e-4;
```

INTERMEDIATE MASS

```
pend.m2_parameters = 'inventor calculated';
pend.material2 = 'aluminium cylinder with central hole';
pend.m2 = 0.873;
pend.l2x = 1.328552e-3;
pend.l2y = 8.17635e-4;
pend.l2z = 8.10443e-4;
```

TEST MASS

```
pend.m3_parameters = 'inventor calculated';
pend.material3 = 'silica';
pend.m3 = 0.846;
pend.l3x = 1.050091e-3;
pend.l3y = 6.98076e-4;
pend.l3z = 7.00937e-4;
pend.tr = 99.6e-3 / 2;
```

SUSPENSION ELEMENTS

```
pend.l1 = 222.8e-3; %0.22;
pend.l2 = 200.8e-3; %0.20;
pend.l3 = 350.01e-3; %0.35;
```

upper wire length
intermediate wire length
lower wire length

```
pend.nw1 = 2;
pend.nw2 = 4;
pend.nw3 = 4;
```

number of wires per stage (2 or 4)

```
pend.r1 = 76.2e-6;
pend.r2 = 50.8e-6;
pend.r3 = 27.6e-6;
pend.r3_parameters = 'C70 Steel Wires';
```

radius of upper wire
radius of intermediate wire
radius of lower wire

```
pend.Y1 = constants.materials.C70Steel.Y;
pend.Y2 = pend.Y1;
pend.Y3 = pend.Y1;
pend.Y3_parameters = 'C70 Steel Wires';
```

BLADES

```
pend.nub = 2;
pend.nlb = 2;
```

number of upper blades
number of lower blades

TOP BLADES

```
pend.mntb1 = (pend.m1 + pend.m2 + pend.m3)/pend.nub;
pend.mnb1 = pend.m1/pend.nub;
pend.blade1.parameters = 'matlab calculated';
pend.blade1.l = 0.18;
pend.blade1.t = 0.8e-3;
pend.blade1.root = 3.5e-2;
pend.blade1.tip = 0.8e-2;
```

total mass per blade
uncoupled mass per blade

UPPER BLADES

```
pend.mntb2 = (pend.m2 + pend.m3)/pend.nlb;
pend.mnb2 = pend.m2/pend.nlb;
pend.blade2.parameters = 'matlab calculated';
pend.blade2.l = 0.12;
```

total per blade
uncoupled mass per blade

pend.blade2.t = 0.8e-3;
pend.blade2.root = 1.8e-2;
pend.blade2.tip = 0.42e-2;

X-DIRECTION SEPARATION

pend.su = 0;
pend.si = 4.25e-3;
pend.sl = 3e-3;

1/2 separation of upper wires
1/2 separation of intermediate wires
1/2 separation of lower wires

Y-DIRECTION SEPARATION

pend.n0 = 40e-3/ 2;

pend.n1 = 0.1;

pend.n2 = -((pend.uy) - (2*(pend.blade2.l + 2e-2)))/2;

pend.n3 = pend.ir-0.0035+0.005;

pend.n4 = pend.tr-0.0035+0.005;

pend.n5 = pend.tr-0.0035+0.005;

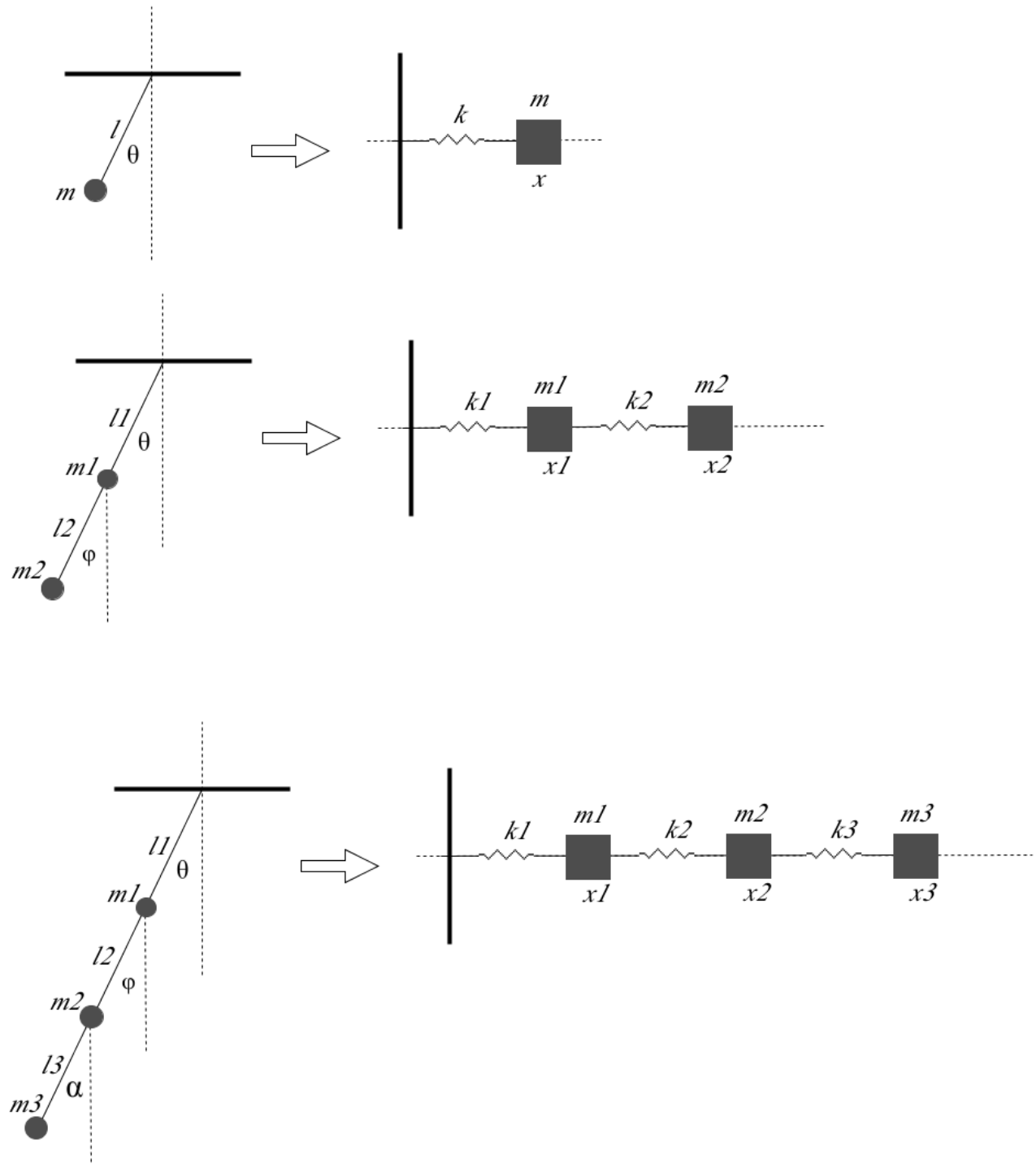
pend.n1 = 55e-3;
pend.n2 = 38.287e-3;
pend.n3 = 56.3e-3;
pend.n4 = 51.3e-3;
pend.n5 = 53.8e-3;

1/2 separation of upper wires at
blades
1/2 separation of upper wires at
upper mass
1/2 separation of intermediate wires
at upper mass
1/2 separation of intermediate wires
at intermediate mass
1/2 separation of lower wires at
intermediate mass
1/2 separation of lower wires at test
mass

D VALUES (geometric)

pend.d0 = 0.072e-3; pend.d0geo = pend.d0;
pend.d1 = 1.128e-3; pend.d1geo = pend.d1;
pend.d2 = 1e-3; pend.d2geo = pend.d2;
pend.d3 = 1e-3; pend.d3geo = pend.d3;
pend.d4 = 1e-3; pend.d4geo = pend.d4;

Appendix B. Single, Double, and Triple Pendulum Calculations



Below are the calculation of the resonant frequencies for single, double and triple pendulum. Wolfram Alpha was used to diagonalize matrices. The following small angle approximations were used in the calculations;

$$\sin\theta = \theta \quad \text{and}$$
$$\theta = \frac{\Delta x}{l}.$$

Single pendulum

The motion of a pendulum at small angles can be described as a simple harmonic oscillator to first order. Thus Hooke's Law for a spring can be used to describe the motion.

By Newton's Second Law

$$F = ma = mx''.$$

By Hooke's Law

$$F = -kx.$$

By Trigonometry (see first figure at beginning of appendix B)

$$F = -mg \sin\theta.$$

Thus

$$mx'' = -\frac{mg}{l}x.$$

The Solution to the Differential Equation is

$$x = e^{i\sqrt{\frac{mg}{l}}x}.$$

The Resonant Frequency is

$$f = \frac{1}{2\pi} \sqrt{\frac{mg}{l}}.$$

Double Pendulum

Referring to the second figure at the beginning of Appendix B, and the calculations for the single pendulum, the following equations for the motion of each mass can be inferred;

$$\begin{aligned} m_1 x_1'' &= -x_1 k_1 + (x_2 - x_1) k_2 \text{ and} \\ m_2 x_2'' &= -(x_2 - x_1) k_2. \end{aligned}$$

These equations can be written as a 2 by 2 matrix. For ease of computation of the matrix the following parameters are used;

$$k_1 = k, \quad k_2 = j, \quad m_1 = m, \quad \text{and} \quad m_2 = n.$$

Below is the Matrix derived from the equation of motion along with it's diagonalization;

$$M = S.J.S^{-1}$$

where

$$M = \begin{pmatrix} \frac{-j-k}{m} & \frac{j}{m} \\ \frac{j}{n} & -\frac{j}{m} \end{pmatrix}$$

$$S = \begin{pmatrix} \frac{-kn - \sqrt{4mj^2 + k^2n}\sqrt{n}}{2jm} & \frac{\sqrt{n}\sqrt{4mj^2 + k^2n} - kn}{2jm} \\ 1 & 1 \end{pmatrix}$$

$$J = \begin{pmatrix} \frac{-2jn - kn - \sqrt{4mj^2 + k^2n}\sqrt{n}}{2mn} & 0 \\ 0 & \frac{-2jn - kn + \sqrt{4mj^2 + k^2n}\sqrt{n}}{2mn} \end{pmatrix}$$

$$S^{-1} = \begin{pmatrix} -\frac{jm}{\sqrt{n}\sqrt{4mj^2 + k^2n}} & \frac{\sqrt{n}\sqrt{4mj^2 + k^2n} - kn}{2\sqrt{n}\sqrt{4mj^2 + k^2n}} \\ \frac{jm}{\sqrt{n}\sqrt{4mj^2 + k^2n}} & -\frac{-kn - \sqrt{4mj^2 + k^2n}\sqrt{n}}{2\sqrt{n}\sqrt{4mj^2 + k^2n}} \end{pmatrix}$$

To more clearly display the features and resonant frequencies for the double pendulum, below is show the case where;

$$k_1 = k_2 \quad \text{and} \quad m_1 = m_2.$$

$$M = S.J.S^{-1}$$

where

$$M = \begin{pmatrix} -\frac{2k}{m} & \frac{k}{m} \\ \frac{k}{m} & -\frac{k}{m} \end{pmatrix}$$

$$S = \begin{pmatrix} \frac{1}{2}(-1 - \sqrt{5}) & \frac{1}{2}(-1 + \sqrt{5}) \\ 1 & 1 \end{pmatrix}$$

$$J = \begin{pmatrix} \frac{(-3 - \sqrt{5})k}{2m} & 0 \\ 0 & \frac{(-3 + \sqrt{5})k}{2m} \end{pmatrix}$$

$$S^{-1} = \begin{pmatrix} -\frac{1}{\sqrt{5}} & -\frac{1 - \sqrt{5}}{2\sqrt{5}} \\ \frac{1}{\sqrt{5}} & -\frac{-1 - \sqrt{5}}{2\sqrt{5}} \end{pmatrix}$$

The eigenvalues of the original matrix are the diagonals of the J matrix

$$\lambda_1 \approx -\frac{2.61803k}{m}$$

and

$$\lambda_2 \approx -\frac{0.381966k}{m}$$

The Resonant Frequencies are the square root of the negative of the eigenvalues divided by two pi;

$$f_1 = \frac{1}{2\pi} \sqrt{\frac{2.61803k}{m}}$$

and

$$f_2 = \frac{1}{2\pi} \sqrt{\frac{0.381966k}{m}}$$

Triple Pendulum

Referring to the third figure at the beginning of Appendix B, and the calculations for the single pendulum, the following equations for the motion of each mass can be inferred;

$$\begin{aligned}m_1 x_1'' &= -x_1 k_1 + (x_2 - x_1) k_2, \\m_2 x_2'' &= -(x_2 - x_1) k_2 + (x_3 - x_2) k_3 \text{ and} \\m_3 x_3'' &= -(x_3 - x_2) k_3.\end{aligned}$$

These equations can be written as a 2 by 2 matrix. For ease of computation of the matrix the following parameters are used;

$$\begin{array}{lll}k_1 = k, & k_2 = j, & k_3 = h, \\m_1 = m, & m_2 = n, & \text{and } m_3 = b.\end{array}$$

The Matrix takes the form;

$$\begin{pmatrix} -\frac{k+j}{m} & \frac{j}{m} & 0 \\ \frac{j}{n} & -\frac{j+h}{n} & \frac{h}{n} \\ 0 & \frac{h}{b} & -\frac{h}{b} \end{pmatrix}.$$

To more clearly display the features and resonant frequencies for the triple pendulum, below is show the case where;

$$k_1 = k_2 = k_3 \text{ and } m_1 = m_2 = m_3.$$

$$M = S.J.S^{-1}$$

where

$$M = \begin{pmatrix} -\frac{2k}{m} & \frac{k}{m} & 0 \\ \frac{k}{m} & -\frac{2k}{m} & \frac{k}{m} \\ 0 & \frac{k}{m} & -\frac{k}{m} \end{pmatrix}$$

$$S = \begin{pmatrix} 1.80194 & -1.24698 & 0.445042 \\ -2.24698 & -0.554958 & 0.801938 \\ 1 & 1 & 1 \end{pmatrix}$$

$$J = \begin{pmatrix} -\frac{3.24698k}{m} & 0 & 0 \\ 0 & -\frac{1.55496k}{m} & 0 \\ 0 & 0 & -\frac{0.198062k}{m} \end{pmatrix}$$

$$S^{-1} = \begin{pmatrix} 0.193842 & -0.241717 & 0.107574 \\ -0.43556 & -0.193842 & 0.349292 \\ 0.241717 & 0.43556 & 0.543134 \end{pmatrix}$$

For the case of the triple Pendulum we inserting the values for Reference Cavity Suspension into our matrix to derive the resonant frequencies for the longitudinal degree of freedom. The parameters are listed below. Using the principle derived for the single pendulum that;

$$k = \frac{mg}{l}$$

The parameters are;

$$l_1 = 0.22\text{m}$$

$$l_2 = 0.20\text{m}$$

$$l_3 = 0.35\text{m}$$

$$m_1 = 1050\text{g} = 1.05\text{kg}$$

$$m_2 = 950\text{g} = 0.95\text{kg}$$

$$m_3 = 850\text{g} = 0.85\text{kg}$$

$$k_1 = \frac{m_1 g}{l_1} = 46.8 \text{ N/m}$$

$$k_2 = \frac{m_2 g}{l_2} = 46.6 \text{ N/m}$$

$$k_3 = \frac{m_3 g}{l_3} = 23.8 \text{ N/m.}$$

The matrix takes the form;

$$\begin{pmatrix} -\frac{46.8+46.6}{1.05} & \frac{46.6}{1.05} & 0 \\ \frac{46.6}{0.95} & -\frac{46.6+23.8}{0.95} & \frac{23.8}{0.95} \\ 0 & \frac{23.8}{0.85} & -\frac{23.8}{0.85} \end{pmatrix}$$

Diagonalizing the matrix gives the following result;

$$M = S.J.S^{-1}$$

where

$$M = \begin{pmatrix} -88.9524 & 44.381 & 0 \\ 49.0526 & -74.1053 & 25.0526 \\ 0 & 28. & -28. \end{pmatrix}$$

$$S = \begin{pmatrix} 0.70758 & 0.576155 & 0.295695 \\ -0.682222 & 0.505342 & 0.530772 \\ 0.18413 & -0.642398 & 0.794257 \end{pmatrix}$$

$$J = \begin{pmatrix} -131.743 & 0 & 0 \\ 0 & -50.0262 & 0 \\ 0 & 0 & -9.28865 \end{pmatrix}$$

$$S^{-1} = \begin{pmatrix} 0.745436 & -0.650272 & 0.157033 \\ 0.64226 & 0.509672 & -0.579703 \\ 0.34665 & 0.562975 & 0.753768 \end{pmatrix}$$

The eigenvalues of the original matrix are the diagonals of the J matrix

$$\lambda_1 \approx -131.743$$

$$\lambda_2 \approx -50.0262$$

and

$$\lambda_3 \approx -9.28865$$

The Resonant Frequencies are the square root of the negative of the eigenvalues divided by two pi;

$$f_1 = \frac{1}{2\pi} \sqrt{131.743} = 1.827 \text{ Hz}$$

$$f_2 = \frac{1}{2\pi} \sqrt{50.0262} = 1.125 \text{ Hz}$$

and

$$f_3 = \frac{1}{2\pi} \sqrt{9.28865} = 0.485 \text{ Hz.}$$